ELSEVIER

Contents lists available at ScienceDirect

Applied Materials Today

journal homepage: www.elsevier.com/locate/apmt



Baicalin-loaded proline and hydroxy proline functionalized chitosan derivative nanofiber composite as burning wound dressings

Azam Sharifi ^a, Sakineh Mashjoor ^{b,c,d,*}, Behzad Sharif Makhmalzadeh ^{a,e,**}, Layasadat Khorsandi ^f, Mohammad Reza Shushizadeh ^{c,d,g}

- ^a Department of Pharmaceutical Sciences, Faculty of Pharmacy, Ahvaz Jundishapur University of Medical Sciences, Ahvaz, Iran
- b Department of Marine Biology, Faculty of Natural Resources and Marine Sciences, Tarbiat Modares University, Noor, Iran
- ^c Department of Marine Pharmacognosy, Faculty of Pharmacy, Ahvaz Jundishapur University of Medical Sciences, Ahvaz, Iran
- ^d Marine Pharmaceutical Science Research Center, Ahvaz Jundishapur University of Medical Sciences, Ahvaz, Iran
- ^e Nanotechnology Research Center, Ahvaz Jundishapur University of Medical Sciences, Ahvaz, Iran
- f Department of Anatomical Sciences, Faculty of Medicine, Cellular and Molecular Research Center, Ahvaz Jundishapur University of Medical Sciences, Ahvaz, Iran
- g Department of Medicinal Chemistry, School of Pharmacy, Ahvaz Jundishapur University of Medical Sciences, Ahvaz, Iran

ARTICLE INFO

Keywords: Regenerative medicine Collagen-based amino acid Electrospinning Nanofibrous dressing Drug delivery Cell therapy Third-degree burn Wound healing

ABSTRACT

Properly managing burn wounds and developing biomimetic dressings to accelerate wound closure and relieve pain are critical healthcare demands. The study focused on designing innovative nanofiber composites for third-degree burn wound recovery using electrospinning techniques. The process involved synthesizing proline (Pr) and hydroxyl proline (HyP) functionalized chitosan (CS) as PHPC, fabricating electrospun nanofibrous based on the PHPC and/or CS, polyvinyl alcohol (PVA), and using the bioactive compound baicalin (BAC) as a loading drug. Mouse Dermal Fibroblast (MDF) cells were then loaded onto the wound-dressing nanoscaffolds to assess their pharmacotherapeutic potential for wound healing in a rat model. The analysis of the scaffold characteristics using FTIR, NMR, DSC, and SEM confirmed the amino acid and drug loading as well as highly nano-porous and network structures (>190 nm). The hydrophilic PHPC-based nanofibrous composities demonstrated enhanced wettability for wound secretions, elasticity, drug release, and cytocompatibility properties compared to CS-based scaffolds. The PHPC/PVA/BAC/MDF also showed a better maturity of the regenerative skin tissues and had a comparable healing effect to control on third-degree burn model, due to their ability to stimulate cell migration/proliferation/re-epithelialization, collagen deposition, and angiogenesis, and alleviate the wound inflammatory phase based on the antioxidant activity of BAC. In conclusion, this novel skin nanofibrous dressing of BAC-loaded cellularized amino acids-based CS derivatives shows promising therapeutic efficacy in burn wound care.

1. Introduction

The skin acts as a protective barrier against injuries and microorganisms, but it is susceptible to damage, which imposes a significant social and economic burden [1]. Burn wounds can cause physically debilitating injuries and affect almost every organ in patients, leading to severe morbidity and mortality. Burn injuries can be categorized based on their severity and depth of skin injury. Superficial burns reach only up to the epidermal surfaces of the skin, causing redness. Partial-thickness burns damage the epidermis and part of the dermis layers of the skin. Third-degree burn wounds are severe injuries, that

destroy almost all the skin layers, which are extremely challenging to manage [2]. Burned patients often need wound dressings that promote the adhesion, migration, attachment, and proliferation of fibroblast cells, as well as support angiogenesis to ensure effective wound healing management, especially when skin autografts are limited [3]. Wound healing is a dynamic and complex process that involves a series of events, including inflammation, cell proliferation, and migration [4] particularly fibroblasts, that play a crucial role in tissue repair by secreting growth factors, cytokines, collagens, and extracellular matrix (ECM) components [5–7]. However, current therapeutic approaches and wound dressings have proven to be consistently inadequate, as they are

^{*} Corresponding author at: Department of Marine Biology, Faculty of Natural Resources and Marine Sciences, Tarbiat Modares University, Noor, Iran.

^{**} Corresponding author at: Department of Pharmaceutical Sciences, Faculty of Pharmacy, Ahvaz Jundishapur University of Medical Sciences, Ahvaz, Iran. E-mail addresses: mashjoor.s@gmail.com (S. Mashjoor), makhmlzadeh@yahoo.com (B.S. Makhmalzadeh).

prone to secondary damage, trapping fluid, allergic reactions, high cost, and infection [8–10]. These limitations demonstrate that existing wound treatments are not effectively addressing the diverse needs of wound healing. A comprehensive understanding of the skin's anatomical structure and function during wound healing, along with a focus on recent advancements in wound treatments utilizing nanotechnology and new biomaterial platforms with antioxidant, anti-inflammatory, and antibacterial properties, is crucial for effective wound management [11, 12].

In the field of Nanomedicine, electrospun nanofiber scaffolds have received significant attention as potential wound dressings due to their unique characteristics, including high oxygen permeability, strong tensile strength, versatile morphological features, tunable porosity, and tailored ability [13,14]. These nanofibers exhibit an extremely high surface-to-volume ratio and high porosity, enabling the creation of highly porous mesh networks with significant interconnectivity, making them appealing for a wide range of advanced applications [15]. The materials used in their production, such as natural polymers, synthetic polymers, carbon-based materials, and semiconductor materials, contribute to these distinctive features [16,17]. Electrospun wound dressings also offer advantages such as hemostatic properties, absorbability, semi-permeability for cell respiration, better conformation to the wound surface, and potential for scar healing [18]. Furthermore, their fine diameter and highly porous structure allow for efficient drug particle dispersion, facilitating high loading and effective drug release from the matrix [19].

Natural polymers such as polysaccharides and proteins found in the ECM have been utilized in the production of wound dressings [20]. Chitosan (CS) and its derivatives, known for being biodegradable, non-toxic, and natural cationic polysaccharides polymers, have shown promise in wound healing due to their film-forming, significant absorbability, antimicrobial, and antioxidant properties [21]. Chitosan is effective for preventing or treating wound and burn infections, not only due to its natural antimicrobial properties but also because it can deliver external antimicrobial agents to wounds and burns [22,23]. Furthermore, it aids in the removal of bacteria from the wound during the inflammation stage. Ultimately, they accelerate skin proliferation by promoting the growth of granulation tissue during the proliferation stage [24]. CS-based nanocomposite films, being thin, flexible, and transparent, are suitable for transferring water vapor, O2, and CO2 in the wound microenvironment, as well as for use in a controlled drug delivery system (DDS) for wound healing [25].

Recently, the poly(vinyl alcohols) (PVA) electrospinning is attracting considerable biomedical research interest because PVA as a water-soluble synthetic polymer bearing CH₂CH(OH) repeating units has shown promise as a biodegradable and cost-effective material for developing a new type of nanofibrous dressing matrix [26]. These bio-inspired platforms can release drugs in a controlled manner, create a moist wound environment, increase drug release and healing rates, and enhance the physical properties of the functional dressing materials [27].

In pharmacological applications, the use of nanocomposite scaffolds has been found to improve the adhesion and development of fibroblast cells in wounds. The combination of polymeric nanofibers with skin fibroblasts accelerates the wound-healing process, shortens the inflammatory phase, and expedites collagen deposition [28]. When tissue damage occurs, fibroblasts play a role in regulating immune cell recruitment, behavior, retention, and survival. Additionally, the interaction between fibroblasts and macrophages is crucial in determining the proper progression of the healing process from the inflammatory phase to the subsequent proliferation phase [28]. In the context of burn wounds, the activation of Mesenchymal cells (MSCs) autophagy in the burn environment regulates the proliferation and migration of burn wound fibroblasts by influencing the production of TGF- β 1 and PGE-2 [29]. This process stimulates myofibroblasts to express α -SMA, transforming them into myofibroblasts, which then undergo apoptosis,

ultimately contributing to the healing process [30]. Ensuring stimulation of fibroblast and collagen biosynthesis is essential for maintaining tissue integrity during wound healing [28].

At present, collagen-based formulations have garnered significant attention as promising materials for treating injuries. Type I and type VII collagen play a crucial role in wound healing as fundamental components of the ECM [31,32]. Collagen, a heterotrimeric protein, consists of two $\alpha 1$ chains and one $\alpha 2$ chain, each with a specific repeating unit [Gly-Xaa-Yaa], where Yaa is primarily L-4-hydroxyproline (HyP) and Xaa is mainly L-proline (Pr). Regulating proline and hydroxyproline can stimulate fibroblast and collagen biosynthesis [32,33]. Collagen possesses various physiological and biological properties, including non-inflammation, high degradability, low antigenic properties, elasticity, softness, flexibility, ability to be grafted to tissue, imperviousness to the entry of bacteria and other pathogens, and non-toxicity, making it widely used in burn repair, drug delivery systems, tissue regeneration, and replacement [34,35]. The use of nanofibrous scaffolds created from natural polymers like polysaccharides, proteins, and various types of collagen has become increasingly desirable in wound healing [36]. However, animal or allogenic collagen proteins have insufficient mechanical properties for tissue engineering and can stimulate the immune system, leading to tissue rejection [37]. This limits the biomedical application of collagen-based scaffolds. To address this challenge, novel degradable polymers, including CS, can be modified by substituting groups of collagen-based amino acids like proline and hydroxyproline, given their multifunctionality, chiral configuration, and easy accessibility for a diverse range of biological and biomedical applications [38-40].

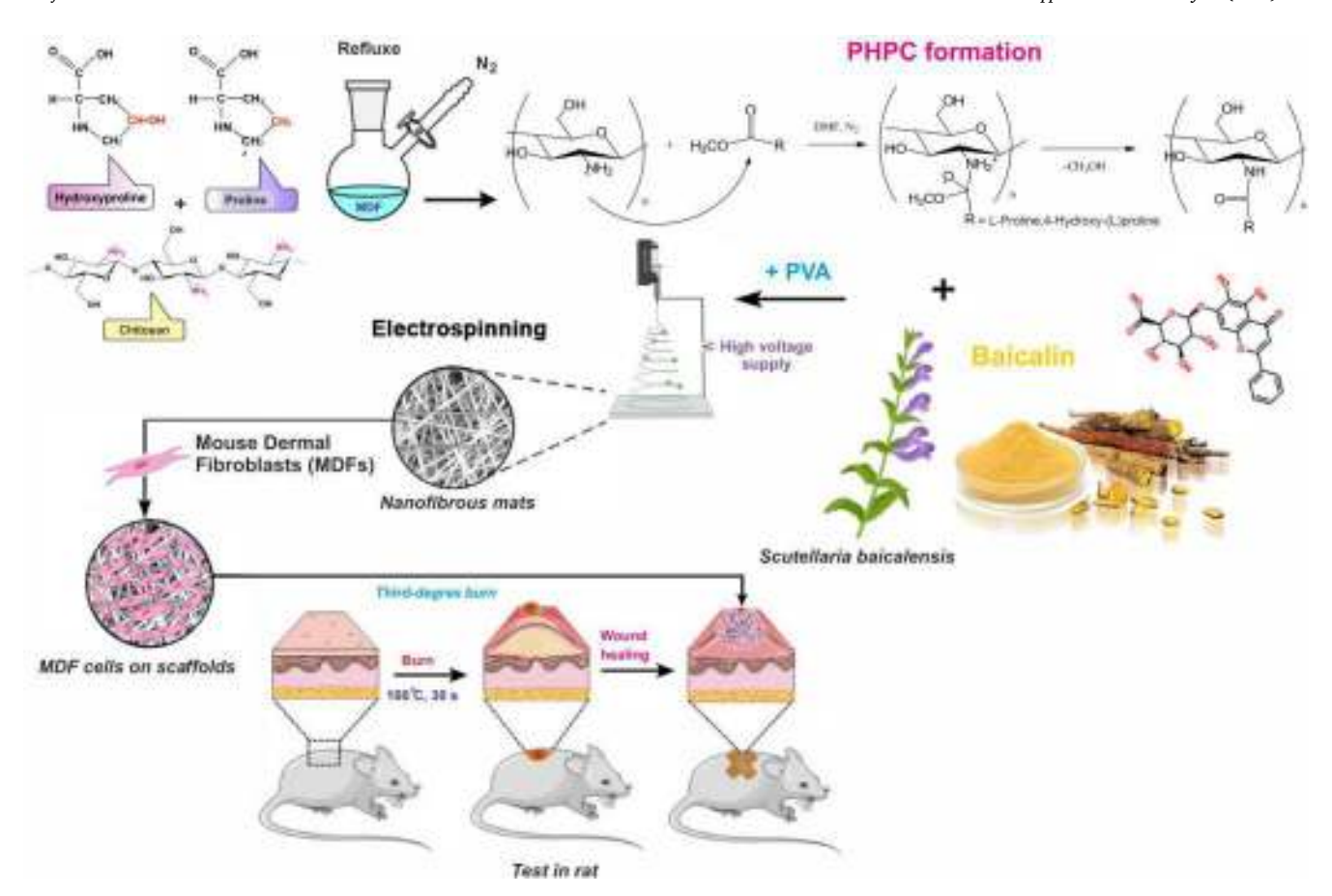
Numerous natural biomaterials have been adopted to improve burn wound healing. One such bioactive substance is Baicalin (BAC) (5,6dihydroxy-2-phenyl-4H-1-benzopyran-4-one-7-O-D-b-glucuronic acid), a plant-derived flavonoid extracted from the Chinese herb Scutellaria baicalensis Georgi (Scheme 1) [41]. Baicalin has shown diverse positive effects on wound healing in various formulations such as nanofibrous and hydrogel [42,43] exhibiting multitherapeutic functions such as anti-oxidative [42] anti-bacterial [43] anti-cancer [44] anti-aging [45] and anti-inflammatory [46] in the field of biomedicine. BAC has been shown to possess immunomodulatory functions, primarily through the inhibition of the NF-κB signaling pathway and NLRP3 inflammasome activation, as well as the suppression of pro-inflammatory factor expression including interleukin (IL)-1 β , IL-6, IL-8, tumor necrosis factor α (TNF-α), cyclooxygenase 2 (COX-2), inducible nitric oxide synthase (iNOS), etc. (Scheme 2) [47]. The therapeutic applications and biological activities of baicalin emphasize its potential for use in wound dressing. However, its poor solubility/hydrophilicity, and bioavailability in water (0.054 mg/ml, $2.2 \pm 0.2\%$, respectively) [48] and low lipophilicity, along with the lack of adequate clinical data and suitable vehicles, currently restrict its use as a medicinal agent [46].

Considering the biofunction of baicalin in inflammatory disease, this study reported a novel approach to syntheses of BAC-loaded Pr/HyP functionalized chitosan derivative nanofiber composite, which serves as a new platform for drug delivery. The electrospun nanofiber scaffolds were created using proline and hydroxy proline derivatives of chitosan (PHPC), polyvinyl alcohol, and baicalin. The effectiveness of these nanofibrous scaffolds was evaluated after introducing fibroblast cells from mice to it and assessing their ability to treat second-degree burn wounds in a rat model.

2. Experimental section

2.1. Materials

All chemicals and materials used in the experiments were: Chitosan (Medium Mw, 85%Deacetylation) (Solarbio, China), L-Proline methyl ester, and L-4-hydroxyproline methyl ester (Sigma Aldrich, Germany), Polyvinyl alcohol, PVA (Average Mw 130,000 g/mol 99+% hydrolyzed)



Scheme 1. A scheme demonstrating how PHPC is formed, the creation of PHPC/PVA/BAC nanofiber scaffolds the loading of MDF cells onto these scaffolds, and our in vivo experimental plan.

(Sigma Aldrich, Germany), Baicalin (FW 446.4) (Sigma Aldrich, Germany), Fetal bovine serum, FBS (Biosera, America), Mouse Dermal Fibroblast, MDF (Royan stem cell bank, Iran), Dulbecco Modified Eagle Medium, DMEM culture (Bio-Idea, Iran), Acridine orange (Sigma Aldrich, Germany), Ethidium bromide (Merck, Germany), Phosphate-buffered saline, PBS (Merck, Germany), Trypsin-EDTA (Bio-Idea, Iran), PEN-STREP 100X (Bio-Idea, Iran), L-glutamine (Bio-Idea, Iran), and Hydroxyproline Assay Kit (Kiazist, Iran).

2.2. Synthesis of Pr and HyP derivatives of CS (PHPC)

The synthesis of PHPC involves modifying the previous protocol to functionalize chitosan with amino acids [58]. Initially, 1 g of chitosan was dissolved in 2% aqueous acetic acid and agitated in a shaking incubator at 30°C, 200 rpm, for 24 hours. The resulting viscous, pale yellow chitosan solution was then filtered at 45 µm to remove any undissolved matter [59]. Afterward, the fabrication of PHPC was conducted in a 250 ml round-bottom flask, where 0.67 g of L-proline methyl ester and 0.67 g of L-4-hydroxyproline methyl ester were dissolved in 30 ml of dimethylformamide (DMF). This mixture was added to the chitosan solution and refluxed under nitrogen gas at 100°C for 3 days [58]. After completing the reaction, the obtained brick-colored mixture was cooled at room temperature. The collected Pr/HyP-functionalized chitosan (PHPC) product was washed with methanol several times to remove impurities and then dried [60]. The PHPC product was neutralized by treating it with 10 ml of 10% NaOH for 15-20 minutes. The PHPC beads were washed with distilled water three times to remove alkaline medium [61]. Finally, the product was placed in a desiccator for three days, and the structure was analyzed using the NMR-FTIR technique.

2.3. Fabrication of PHPC/PVA/BAC

The fabrication of CS/PHPC-loaded PVA nanofiber mats was carried out using the electrospinning method, following a previously described procedure [60]. To summarize, 10% (w/v) PVA was dissolved in deionized water and stirred at 90°C for 1 hour at a constant temperature [62]. After cooling the PVA solution to 25°C, 1.25% (w/v) PHPC and/or CS was dissolved in a 1% (v/v) acetic acid solution (0.5 M) and slowly added to the mixture, which was then stirred for 12 hours at room temperature (25°C). Subsequently, a BAC suspension with a concentration of $100 \mu M$ was added to the mixture and stirred for 0.5 hours at room temperature. The chosen BAC concentration was determined based on pre-formulation studies [63] and our and other previous cytotoxicity assessment [64-66] to ensure its suitability and safety for the DDS. To improve the solubility of BAC, the BAC powder was dissolved in a solution of 25% EtOH and ddH2O. A two glass syringe was filled with 10cc of the spinning polymer solution and connected to a stainless steel needle with an inner diameter of 0.9 mm. This needle was then linked to the emitting electrode of a Gamma High Voltage Research device with a positive polarity. The rotation speed of the drum was set at 100 rpm, the distance between the needle and the drum was 15 cm, the solution discharge speed was 2 ml/h, and the voltage was set between 14-18 kV at room temperature. After collecting the electrospun nanofiber mats (5 \times 15 cm) on an aluminum foil-covered rotating collector, they were left under vacuum at 40°C overnight to eliminate any residual solvent. Following this, the mats underwent a crosslinking treatment with NH4+ vapor for 4 hours, and then they were irradiated with UV light for 10 minutes.

2.4. Characterization of nanofiber scaffolds

241 SEM

The surface morphology of the nanofiber scaffold samples was examined using a scanning electron microscope (LEO/ZEISS 1455VP SEM, Germany). The nanofiber scaffolds were sectioned and coated with a thin layer of gold. Subsequently, measurement software was utilized to determine the diameter and thickness of selected fibers, and their average values were calculated.

2.4.2. DSC

Thermograms of samples (5 mg) containing BAC powder and BAC loaded into the CS and PHPC nanofibers were analyzed using a differential scanning calorimetry (DSC) machine. The analysis was performed at a speed of 10° C/min within a temperature range of -50 to 250° C.

2.4.3. FT-IR

The structural changes in the nanofibers before and after the addition of BAC were assessed using a Fourier transform infrared (FTIR) spectrometer (Bruker's VERTEX 70v FT-IR, Germany). The FTIR spectra of the nanofibers were recorded in the range of 4000-500 nm to identify the functional groups.

2.4.4. Tensile strength

Samples with specific dimensions (60×20 mm) were cut from the nanofibers for the assessment of their tensile strength. A Texture analyzer device (STM-20; SANTAM, Iran) was utilized for this purpose. The procedure involved setting the distance between the jaws to 30 to 40 mm, applying weights of 1 to 5 kg, moving the jaws at a speed of 5 mm/s, and plotting the results on a graph.

2.4.5. Drug release

The study utilized a beaker equipped with a mesh wall and a stirrer. Nanofibers of specific dimensions (60×30 mm) were placed into the beaker wall, which was filled with 10 ml of phosphate buffer (PBS) with a pH of 7.4. The beaker was continuously agitated at 150 rpm in an incubator set at 37° C. The percentage of drug (BAC) release was monitored at 1, 3, 5, 8, 24, 48, and 72-hour intervals. Following this, the supernatant was collected, centrifuged at 4000 rpm for 10 minutes, and its absorbance was measured at 259.5 nm using a spectrophotometer (PerkinElmer Inc., MA, USA). The cumulative BAC release data were then analyzed and fitted to different release kinetic models, including zero order, first order, and Higuchi's model [67].

2.4.6. Water vapor permeability (WVP)

To measure water vapor permeability (WVP), the scaffolds were positioned in flexible-capped permeation bottles and incubated at 33°C for 12 hours. WVP at steady-state was calculated using Eq. (1):

$$WVP = \frac{W}{AT} \tag{1}$$

where W represents water lost, A denotes the scaffolds area (1.22 cm²), and T signifies the exposure time.

2.4.7. In vitro degradation of scaffold

To assess the degradation of nanofibrous scaffolds over time, individual scaffolds (2.5 \times 2.5 cm) were immersed in PBS solution. Six specimens of each type of nanoscaffold were grouped, and their average initial weight (W_0) was determined after multiple weighings. These scaffold groups were then placed in a cell culture-mimicking environment in an incubator (37°C, 5% CO₂). After 7 and 14 days, one group of scaffolds was taken out, dried in a vacuum for 48 hours, and reweighed (W_1) to calculate the weight loss using the Eq. (2):

$$weightloss(\%) = \frac{W0 - W1}{W1} \times 100 \tag{2}$$

where W_0 and W_1 represent the weights before and after degradation time t, respectively.

2.4.8. Wettability analysis

The scaffolds' water contact angle (WCA) was measured using a contact angle goniometer (Jikan CAG-10, Iran). A 10 μl drop of pure water was deposited onto the nanofiber scaffold surfaces, and the alteration in WCA over time was documented.

2.4.9. Swelling ratio

To measure the swelling ratio, a specific amount of nanofiber is weighed and then immersed in 2 ml of phosphate buffer with a pH of 7.4. Every hour, the liquid surrounding the nanofiber is dried, reweighed, and then returned to the buffer. This process is repeated for up to 4 hours, and the swelling percentage is calculated using the following Eq. (3):

% swelling =
$$(M - Md)/Md \times 100$$
 (3)

Here, M and Md represent the weight before and after swelling, respectively.

2.4.10. Drug content

In this experiment, the total drug content (BAC) and its uniformity throughout the nanofibers are evaluated using an ultraviolet-visible detector. Samples measuring 4 \times 2 cm are cut from each film and immersed in 10 cc of PBS solution (pH 7.4) to assess baicalin solubility in aqueous buffers. The mixture is continuously shaken at 150 rpm in an incubator at 37°C for 24 hours to allow complete dissolution of BAC. Subsequently, the solution is separated, centrifuged at 4000 rpm for 10 minutes, and the absorbance of the supernatant is measured at a wavelength of 259.5 nm.

2.4.11. Mucoadhesive properties

The mucoadhesive force of nanofiber scaffolds on sheep buccal mucosa was evaluated using a texture analyzer equipped with a 50-N load cell. A 60×20 mm nanofiber sample was tested for its ability to adhere to the sheep's mucous membrane at 37° C in a simulated saliva solution. The tissue was secured onto the holder, and 500μ L of artificial saliva was applied to the center of the mucosa. Initially, a constant force (3g) was applied for 1 minute, and then the mucoadhesive property was determined by measuring the detaching pressure.

The force was calculated using the following Eq. (4):

$$F = (Ww \times g)/A \tag{4}$$

where Ww represents the weight required for separation, g is the gravitational acceleration, A is the nanofiber surface area, and F denotes the adhesion force.

2.5. Cell culture

2.5.1. Sterilization of nanofibrous scaffolds

Nanofibrous scaffolds sterilization process involved cutting the scaffolds into 2.5×2.5 cm sections, followed by simultaneous UV-C and UV-B light exposure for 30 minutes on each side. Subsequently, a salt hydroalcoholic solution (EtOH-PBS) was used for film sterilization. The sterilized slices were then placed in each well of a 24-well plate and treated with 70% ethanol/30%PBS, incubated overnight, washed with sterile PBS, and allowed to dry in the incubator for one hour. Following this, 20 microliters of FBS serum were introduced onto the scaffolds, and they were placed in an incubator for 15 minutes to allow the surface of the fibers to become sticky for cell settlement, followed by cell seeding.

2.5.2. Loading fibroblasts on the surface of nanofibrous mat

We sourced Mouse Dermal Fibroblast (MDF) cells from the RSBC bank, and cultured them in DMEM high glucose medium supplemented

with 10% FBS, 2 mM L-glutamine, 100 Uml⁻¹ penicillin, 100 pg ml⁻¹ streptomycin. The cells were then incubated at 37°C in a humidified atmosphere with 5% CO2 and 95% O2 until they reached the desired cell density of 85%. Once the cells had been passed 4 to 5 times in the T25 cell flasks, the fibroblasts underwent trypsinization, centrifugation, and were collected in DMEM. After re-suspension in culture medium and counting using a hemocytometer, they were seeded onto the scaffolds at a concentration of 10⁵ cells/well. In this study, 20 microliters of the cell suspension were placed on the center of the outer side of the cut crosssection of the nanofibers in each well of the 24-well plate. After a15minute incubation, 1 ml of DMEM medium was slowly added to the plate, and the cells were then left to incubate at 37°C for 24 hours, allowing them to diffuse into and adhere to the surface of the fibers. Subsequently, the cells were observed under the microscope, and again 1 ml of DMEM medium was added to the plate the next day to facilitate continued cell growth. Following 48 hours of cell seeding, the nanofibrous scaffolds containing MDF cells were deemed ready for transfer to the wound surface of rats and dressing [68]. It's worth noting that in this section, some experimental limitations were encountered: i) limited cell infiltration from the sides of each layer of the nanofiber film. To circumvent this, 20 microliters of the cell suspension were loaded on the inner side of the cut cross-section of the nanofiber scaffolds 24 hours before the film was placed on the wound. ii) changes in the size of the cell-hybrid scaffolds (2.5 \times 2.5 cm) soaked in MDF cell culture medium, resulting in a final size of 1.5×1.5 cm for placement on the wound. Therefore, for the other nanofiber scaffold groups without cell-loading, final sizes of 1.5×1.5 cm were used.

2.5.3. SEM imaging of cell

To image the MDF cells using scanning electron microscopy (SEM), the cultured cells on nanofibrous scaffolds were first fixed with a 2.5% glutaraldehyde solution in PBS for 2 hours, followed by three washes in PBS. Subsequently, the nanofiber structures underwent a dehydration process through serial dilution of 30, 50, 70, 80, 90, and 100% of absolute ethanol in PBS at a temperature of 25°C for 10 minutes in each dilution. Following this, the samples were freeze-dried for 12 hours in a freeze dryer (Alpha 1–2 LP plus). The dried scaffold samples were then sputter-coated with gold and imaged with an LEO 1455VP SEM to visualize cells on the fiber and porous structure.

2.5.4. MTT assay

The MTT Assay was used in this study to analyze MDF cell viability after 24 hours of BAC exposure [69]. A 100 mM BAC concentrate was prepared by dissolving 44.64 mg baicalin in 1 ml dimethyl sulfoxide (DMSO), which was then diluted to create the required BAC working solution. Cells in the logarithmic growth phase were seeded in 96-well plates (5 \times 10 3 cells per well), cultured overnight, and then treated with different concentrations of baicalin (0, 25, 50, 75, 100, and 125 μ M). After 24 hours, the MTT (3-(4,5-dimethylthiazol-2-yl)-2,5-diphenyltetrazolium bromide) solution (10 μ l/100 μ l in fresh medium) was added, and after further incubation of 4 hours at 37°C, the medium was aspirated and the wells washed with PBS. Then, the wells were dried for 2 hours, and in the next step, 200 μ l of DMSO was added to each well. To dissolve the dye, the microtitre plate was placed on a shaker, and the optical density (OD) value was measured at 570 nm to calculate the % viability based on Eq. (5).

% Viability = (Mean assay absorption test / Mean negative control absorption)
$$\times$$
 100 (5)

2.5.5. Cytocompatibility assay

The cytocompatibility of CS/HA/PVA and PHPC/HA/PVA nanofiber scaffolds was assessed using the MTT test, comparing them to control with fibroblasts seeded in a well plate without nanofibers. The nanofibers were placed in 96-well plates, and fibroblast cells were seeded and then incubated at 37°C and 5% Co $_2$ for 24 and 48 hours. Five ml of MTT

solution was dissolved in one ml PBS and then added to wells and incubated for 4 hours, followed by treatment with DMSO. The optical density was read at 570 nm using an Elisa Reader.

2.5.6. DAPI staining

For the DAPI staining, one day after cell seeding, the morphological changes of the MDF cells on nanofibrous scaffolds in a 24-well plate were examined. The cell culture wells were washed with PBS, fixed with 4% paraformaldehyde, and stained with DAPI (1 $\mu g \ ml^{-1}$) for 5 minutes. The stained cells were washed three times with PBS and observed/photographed under an inverted fluorescent microscope (Olympus).

2.5.7. Dual AO/EB staining

In this study, after two days of cell culture on the fiber surface in 24-well plates, the fluorescent double staining method of acridine orange/ethidium bromide (AO/EB) was used for the cell viability assay. To do this, 0.1 mg of each dye of AO and EB were dissolved in one milliliter of PBS saline buffer inside a microtube to obtain a concentration of 100 μg ml $^{-1}$, and the microtubes were covered with aluminum foil. The cell culture wells were then stained with a dye mixture (10 μl of each dye) and kept inside the incubator in the dark for 10 minutes. Subsequently, the wells were washed with PBS and observed and photographed by an inverted fluorescent microscope (Olympus). Live cells with complete nuclei appeared green, while dead or damaged cells with light or cloudy nuclei appeared red to orange in color [70].

2.6. In vivo test

In the in vivo assessment, the research procedures were authorized by the Ahvaz Jundishapur University of Medical Sciences (IR.AJUMS. ABHC.REC.1401.087) and followed the National Research Council's Guide for the Care and Use of Laboratory Animals [71] 35 adult male Wistar rats, averaging $220\pm35g$ in weight, were employed for the study. The rats underwent a one-week acclimatization period in a room set at $22\pm2^{\circ}\text{C}$ temperature, $55\pm10\%$ humidity, with a 12-hour light-dark cycle. Throughout the experiment, the rats received special compressed food capsules and had unrestricted access to water. To establish burn wounds, the rats were anesthetized with ketamine (50 mg/kg) and xylazine (5 mg/kg) via intraperitoneal injection. A 450 mm² circle was marked on the backs of the rats, and the hair was shaved and disinfected using 70% alcohol. A custom metal iron bar (ϕ = 20 mm), boiled in hot water at 100°C for over 10 minutes, was pressed onto the rats' backs for 30 seconds to induce full-thickness third-degree burn wounds. After disinfecting the wounds with 75% alcohol, each rat was housed in a separate cage. The rats were split into 7 groups, each consisting of 5 individuals, and each group's wounds were treated with different formulations. The groups were as follows: 1st groups: control, 2nd groups: CS/PVA nanofibers, 3rd groups: PHPC/PVA nanofibers, 4th groups: CS/PVA/BAC nanofibers, 5th groups: PHPC/PVA/BAC nanofibers, 6th groups: CS/PVA/BAC/MDF nanofibers, 7th groups: PHPC/PVA/-BAC/MDF nanofibers. Untreated wounds were utilized as a control group. All wound surfaces were covered with transparent stickers and bandaged with pressure-sensitive tape to prevent external contact. At the conclusion of the experiment, the animals were humanely euthanized using the retroorbital ketamine-xylazine method, following the AVMA Guidelines on Euthanasia [72].

Macroscopic Evaluation: The diameter of the wounds was measured daily, and the closure, contraction, and re-epithelialization percentages were determined by analyzing photographs taken during surgery (Day 0) and at 3, 7, and 14 days post-injury. Image J software and digital images were used to analyze the wound healing process. The original wound area was denoted as A, the re-epithelialized skin area as B (thinner), and the remaining open wound as C. The total wound closure (%TWC) was calculated as C/A \times 100%, the contraction contribution to wound closure (%WCC) was calculated as (A-B)/A \times 100%, and the reepithelialization contribution to wound closure (%WCR) was calculated

as $(B-C)/B \times 100\%$ [73,74].

Microscopic Evaluation: On the 7th and 14th days post-wounding, two rats from each group were euthanized using a high dose of ketamine, and tissue samples were collected for histological examination of the wounds.

2.7. Histopathology

After fixation in a 10% formalin buffer solution, the excised skin tissue was processed by rinsing, dehydration, and paraffin embedding. Sections were stained with hematoxylin and eosin (H&E) and then photographed at $100 \times \text{magnification}$.

2.8. Hydroxyproline content

To evaluate the progress of wound healing, the hydroxyproline content in the rat skin wounds was measured on the 14th day using a commercial assay kit (Kiazist Co., Product ID: KHPA96, Tehran, Iran) following the manufacturer's protocol. Hydroxyproline, a key component of collagen, serves as a reliable marker for assessing collagen deposition in granulation tissue [75].

2.9. Statistical analysis

The data were expressed as the mean and standard error of the mean. Statistical analyses were performed using SPSS version 21.0 (SPSS Inc., Chicago, Illinois, USA), utilizing one-way ANOVA testing with a post hoc test. A significance level of *p < 0.05 was considered statistically significant.

3. Results and discussion

3.1. Characterization of PHPC

The process for chemically modifying chitosan with proline and hydroxyproline to synthesize PHPC is illustrated in Scheme 1. The NH₂ functional group in CS reacted with esterified collagen-based amino acids, resulting in the formation of Pr/HyP-functionalized chitosan (PHPC). The mechanism followed was by a nucleophilic attack through the nitrogen of the primary amine group of the chitosan chains and completed with the terminal carboxyl group present in amino acids, which is the result of the formation of amide [58]. This reaction disrupted the regularity and crystallization of the chitosan molecular chain, leading to improved water solubility [76]. The FT-IR and ${}^{1}\text{H}/{}^{13}\text{CNMR}$ results indicated the formation of a new structure (Fig. S1A-C). For unmodified CS, bands at 1641 cm⁻¹ correspond to the C=O group derived from residual N-acetyl groups, 1324 cm⁻¹ to -CH₃ group from residual N-acetyl group, and 1234-896 cm⁻¹ indicate sugar ring vibrating and glycoside bond. In the case of PHPC, the most significant change in the bands compared to CS is in the range of 1750-896 cm⁻¹, and the formation of the carbonyl group at 1654 cm⁻¹ has been observed (Fig. S1A). The modification of chitosan using amino acids, forming PHPC, has been found to enhance the mechanical strength, thermal stability, and chemical stability of the resulting novel material [77,78]. Based on the following results, PHPC has been confirmed as a potential chitosan derivative biomaterial for delivering low-solubility drugs (BAC). The hydroxyl groups located at the 4'-position of the C ring in flavonoid molecules carry high net negative excess charges, whereas the B rings display small positive excess charges [79]. These sections of the molecules are particularly prone to electrophilic attack, making them attractive targets for PHPC. In view of the degradability of CS derivative, PHPC can be digested by cells during the wound-healing process due to the presence of amino acids that are part of the normal metabolic components of living tissues, such as collagens, gelatin, and other proteins. This characteristic is further confirmed by swelling results, making PHPC capable of readily absorbing water and/or wound exudate and

being hydrolytically dissolved.

3.2. Characterization of nanofiber scaffolds

3.2.1. Morphology

The scanning electron microscope (SEM) analysis showed that all the scaffolds exhibited nanofibers with sizes below 200 nm and had a porous, non-woven, and smooth surface morphology, resulting in a high surface area (Fig. 1). Specifically, the CS/PVA/BAC and PHPC/PVA/BAC scaffolds had average nanofiber diameters of 188.9 nm and 174.2 nm, respectively. Notably, the PHPC-based scaffolds produced nanofibers with a smaller diameter than the CS-based scaffolds (Fig. 1). The porous structure, interconnection size, and degree (interconnectivity) of the scaffolds are critical factors in determining their suitability for specific applications such as angiogenesis and wound healing [78,80].

3.2.2. Mechanical property

In this study, we used mechanical properties such as thickness and tensile strength to assess the interactions between a drug and a polymer in a nanofiber scaffold containing the hydrophobic small molecule BAC. Tensile strength (MPa), modulus (MPa), and elongation at the break (%) values for various scaffolds are provided in Table 1 and Fig. S2. The thickness analysis results revealed similar thicknesses for chitosan and PHPC nanofilms (P>0.05). The addition of baicalin to blank films increased the thickness of the nanofibers, although this difference was not significant (p>0.05). The blank PHPC scaffold (PHPC/PVA) exhibited lower tensile strength and modulus but higher elongation at the break values compared to the blank CS scaffolds (CS/HA/PVA). Incorporating proline and hydroxyproline into the CS reduced physical interchain interference and improved elongation at the break (%) values of the scaffolds. However, it seems that PHPC film had better elasticity than chitosan nanofibers, as the addition of collagen-based amino acids reduced the resistance of PHPC nanofibers to tensile stress. Although the mechanical properties of the mats were influenced by the inclusion of BAC and tensile strength slightly decreased in both CS/PVA/BAC and PHPC/PVA/BAC scaffolds (P<0.25), as per a previous report [81]. BAC loading had no adverse effect on the crosslinks and interchain connections in the structure of chitosan derivatives and the overall mechanical properties of the nanofibrous dressing.

3.2.3. WVP property

The effectiveness of wound dressings in retaining moisture and promoting cell growth depends largely on how well nanofiber scaffolds transmit water vapor [82,83]. Based on the information in Table 1, the incorporation of BAC into CS/PVA and PHPC/PVA scaffolds resulted in a reduction of their WVP. The findings suggest that PHPC/PVA/BAC exhibited a significantly lower WVP than the CS/PVA/BAC scaffold (P=0.030). It seems that a PHPC/PVA/BAC scaffold with lower WVP may be more effective in preventing dryness and sustaining proper moisture and oxygen levels necessary for optimal wound healing, as compared to the CS/PVA/BAC scaffold.

3.2.4. WL analysis

The degradation rate of the scaffolds is illustrated by the percentage of weight loss over the incubation time in the PBS solution at 37 °C (Table 1). The results indicate that CS/PVA showed higher degradation resistance than PHPC/PVA. These findings can be attributed to the amidation reaction and the grafting of Pr-Hyp amino acids onto chitosan chains, leading to improved contact angles and intermolecular interactions, transforming the performance from hydrophobic to hydrophilic, which gives the polymer a positive charge, making it easier to disperse [61]. Additionally, the presence of C=N groups in PHPC films enhanced the water solubility of chitosan. At the same time, adding BAC reduced the degradation rate of dissolved scaffold components, potentially due to its lower water permeation rate and lipophilic nature. CS/PVA/BAC and PHPC/PVA/BAC scaffolds exhibited biodegradable

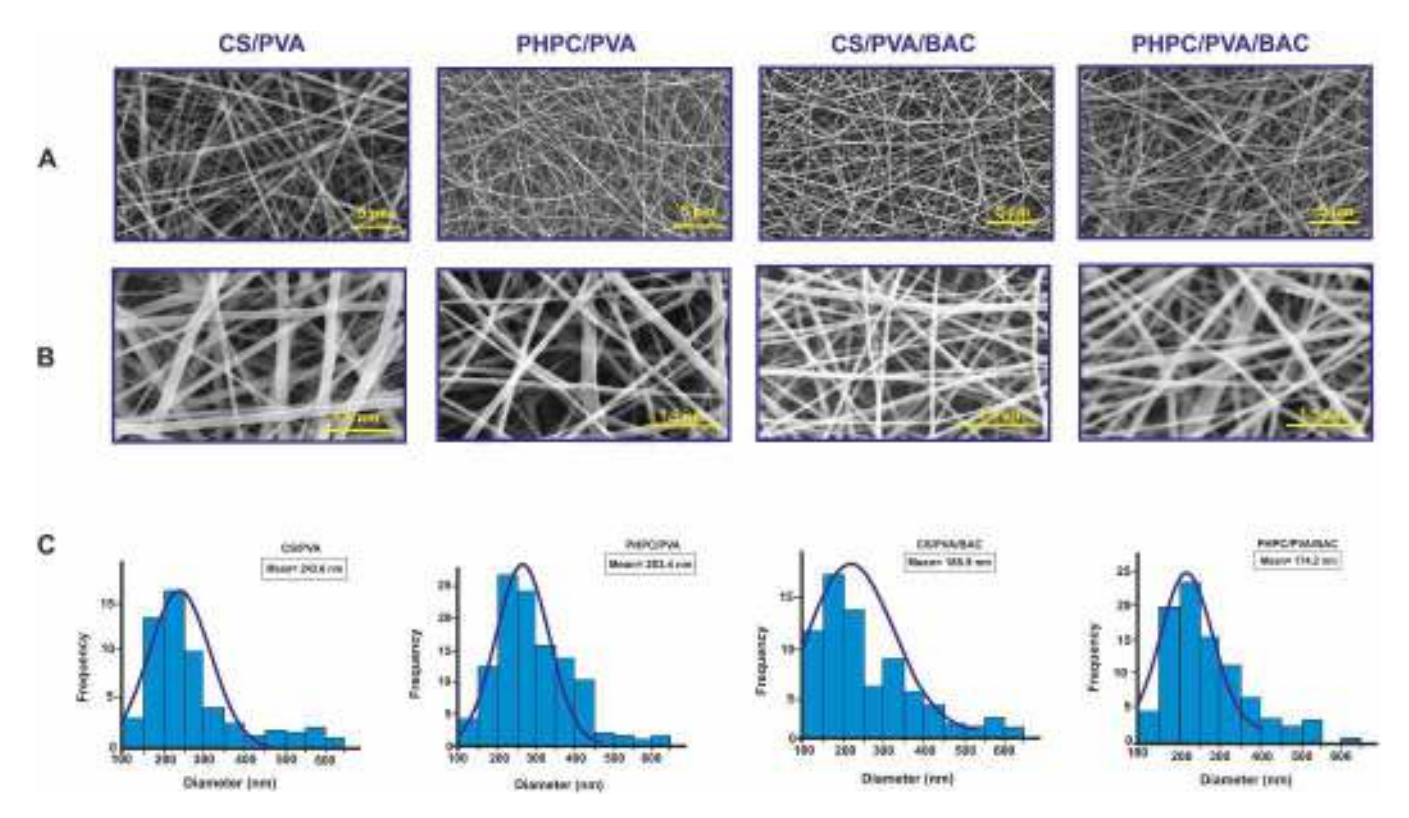


Fig. 1. SEM images of CS/PVA, PHPC/PVA, CS/PVA/BAC, and PHPC/PVA/BAC nanofiber scaffold (A) and its fibrous structure (B), and average diameter comparison (C) (n=100).

Table 1 Characterization of negative control, PHPC and CS blank, and BAC loaded-scaffolds.

Scaffold	Nanomat thickness (μm)	Tensile strength (MPa)	Elongation at break (%)	WVP (mg/cm ² /h)	Weight loss (%)		Swelling (%)	Mucoadhesive force (g)
					Day 7	Day 14		
CS/PVA	8.21±0.9	46.80±3.7	13.60±1.1	12.28±2.5	23.17 ±1.3	37.11 ±1.8	34.70±2.6	21.20±1.6
PHPC/PVA	$8.82{\pm}1.1$	22.91 ± 1.2	$22.50{\pm}2.9$	$11.80{\pm}1.6$	29.14 ±0.9	42.10 ± 1.5	72.36 ± 8.1	28.71 ± 2.1
CS/PVA/BAC	$8.91 {\pm} 0.6$	45.6±3.5	$11.61 {\pm} 1.8$	$11.90{\pm}2.3$	19.23 ± 2.1	25.13 ± 1.6	28.60 ± 3.3	$15.22{\pm}1.3$
PHPC/PVA/ BAC	9.31±0.7	$18.20{\pm}1.3$	$19.32{\pm}0.9$	$10.59{\pm}1.8$	$\begin{array}{c} 24.28 \\ \pm 1.8 \end{array}$	$\begin{array}{c} 33.12 \\ \pm 1.2 \end{array}$	60.8±4.3	$20.30{\pm}2.6$

properties suitable for effective wound dressing.

3.2.5. Wettability and swelling property

The ability of nanofibers to absorb wound exudates is crucial for the wound healing process. The wettability and swelling outcomes of all prepared films are detailed in Fig. S3, and Table 1. The WCA of the nanofibrous membrane surfaces were measured to assess their hydrophilicity. According to Fig. S3, the nanocomposite containing hydrophilic amino acids demonstrated improved wettability compared to the CS-based counterpart. Specifically, the contact angles for CS/PVA and PHPC/PVA were $95.3^{\circ}\pm3.2^{\circ}$ and $53.5^{\circ}\pm1.2^{\circ}$, respectively. Upon the introduction of BAC into both matrices, the surfaces of the nanofibrous membranes shifted towards hydrophobicity, aligning with previous reports [43]. The swelling findings revealed that PHPC-based scaffolds, specifically PHPC/PVA and PHPC/PVA/BAC nanofibers, exhibited superior swelling ratio and water absorption, which was twice as high as their CS-based counterparts, CS/PVA and CS/PVA/BAC nanofibers, creating a hydrated environment conducive to wound healing. Interestingly, adding BAC to the nanofibers did not result in any significant changes in the swelling ratio. Despite BAC being hydrophobic, the nanofilms still displayed effective water absorption, which can be attributed to the presence of CS and its derivative, PHPC, as the biopolymers constituting the films. The presence of amino acids such as Pr and HyP, as water-soluble nitrogen-containing compounds in PHPC, significantly influences the hygroscopic nature of other inorganic compounds in nanofibrous mats [84] and by increase in protein-water hydrogen bonds, the water-absorbing capabilities and elasticity were enhanced [85]. These results suggest that the interactions between PHPC components within the nanofibers greatly impact the water uptake properties of particle mats, leading to controlled release of therapeutic BAC, and improved dressing adhesion.

3.2.6. Mucoadhesive property

Chitosan and its derivatives have a positive charge due to the amine group, allowing them to bind with negatively charged components of mucus and epithelial surfaces. This property could aid in developing a more effective mucoadhesive DDS with a suitable therapeutic moiety for treating oral disorders [86]. In Table 1, an additional test was conducted

to broaden the application and improve the efficacy of baicalin in BAC-loaded CS/PHPC nanofiber mats for topical oral wound dressing [87,88]. The results showed that the force required to separate the PHPC/PVA nanofiber scaffold from the tongue was significantly higher than that of the CS/PVA (P≤0.05). However, the addition of BAC significantly decreased the mucoadhesive properties in both PHPC/PVA/BAC (P=0.033) and CS/PVA/BAC scaffolds (P=0.035) due to BAC's poorly hydrophilic and lipophilic compound nature. Baicalin's basic structure includes a benzopyran ring and a phenolic moiety forming an anomeric linkage with a glucuronic acid moiety, making the molecule soluble in polar protic solvents. It has a Log P value of 1.1, indicating poor lipophilicity. The molecule's main property is the presence of a di-hydroxylated (catechol) substitution on ring A, characteristic of active redox polyphenolic compounds, making them promising materials for oral administration [89]. Although the findings suggest that the addition of BAC may impact the physical properties of the CS/PHPC nanoscaffolds, it can still serve as an effective drug delivery system for maxillofacial surgery [90,91]. The promising wound dressing PHPC/PVA/BAC exhibits biocompatible and biodegradable properties that enhance the oral bioavailability of BAC and its effectiveness on wounds. Pr/HyP is rapidly metabolized within the wound skin [92] and PVA can degrade by PVA oxidases/hydrolases enzymes through interactions with oral symbiotic microbiota [93] while chitosan can be easily broken down inside the human body through enzymatic hydrolytic degradation mechanisms, specifically those involving lysozymes [94,95]. Nevertheless, the literature suggests that modifying chitosan by incorporating sodium alginate (ALG), polyethylene glycol (PEG), and thiol groups can significantly enhance its mucoadhesive properties compared to unmodified chitosan [96,97].

3.2.7. FT-IR of nanofiber scaffolds

The interaction between the different components and BAC during the electrospinning procedures was evaluated using FTIR spectra (Figs. 2 and S1A). In the CS/PVA and PHPC/PVA blank films, various peaks were observed, including a broad peak at 3337–3454 cm⁻¹ related to O-H and amine N-H symmetrical vibration, as well as the intra- and intermolecular hydrogen bonds. The peaks at 2923–2873 cm⁻¹ are related to C-H asymmetric and symmetric stretch vibration from CH2 and CH groups. The band at 1637–1644 cm⁻¹ is linked to water molecules that are associated with the C-OH from the glycosidic units of polysaccharide chains, as well as the presence of residual N-acetyl groups (C=O stretching of amide I), and N-H in plane deformation coupled with C-N stretching of amide II from CS. The bands from 1425–1444 cm⁻¹ are related to CH₂ deformation groups, while the band at 1384 cm⁻¹ corresponds to -CH₃ symmetric deformation, and the bands at 1334-1338 cm⁻¹ are associated with C-N bond stretching of amide III. The band at 1154 cm⁻¹ is attributed to the glycosidic linkage, and the absorption bands in the range 1083–883 cm⁻¹ belong to the C–O–C glycosidic ring (skeletal vibration involving the C-O stretch). The increase in the intensity of the bands from 2923 cm⁻¹ (CH₂ groups), 1450–1437 cm⁻¹ (CH₂ bonds), and at 854–853 cm⁻¹ (NH groups) in the spectrum of CS and PHPC blank films confirms the covalent cross-linking. In the case of BAC-loaded CS/PVA/BAC and PHPC/PVA/BAC scaffolds, the peaks at 3445 and 3337 cm⁻¹ indicate the O–H stretching of the BAC molecule. The appearance of C=O stretching vibration peaks of the carboxyl group at 1735 cm⁻¹ confirms the successful synthesis of the acidic intermediate. The free BAC spectrum demonstrated absorption peaks at 1660 cm⁻¹ and 1496 cm⁻¹, which are related to aromatic bending and stretching

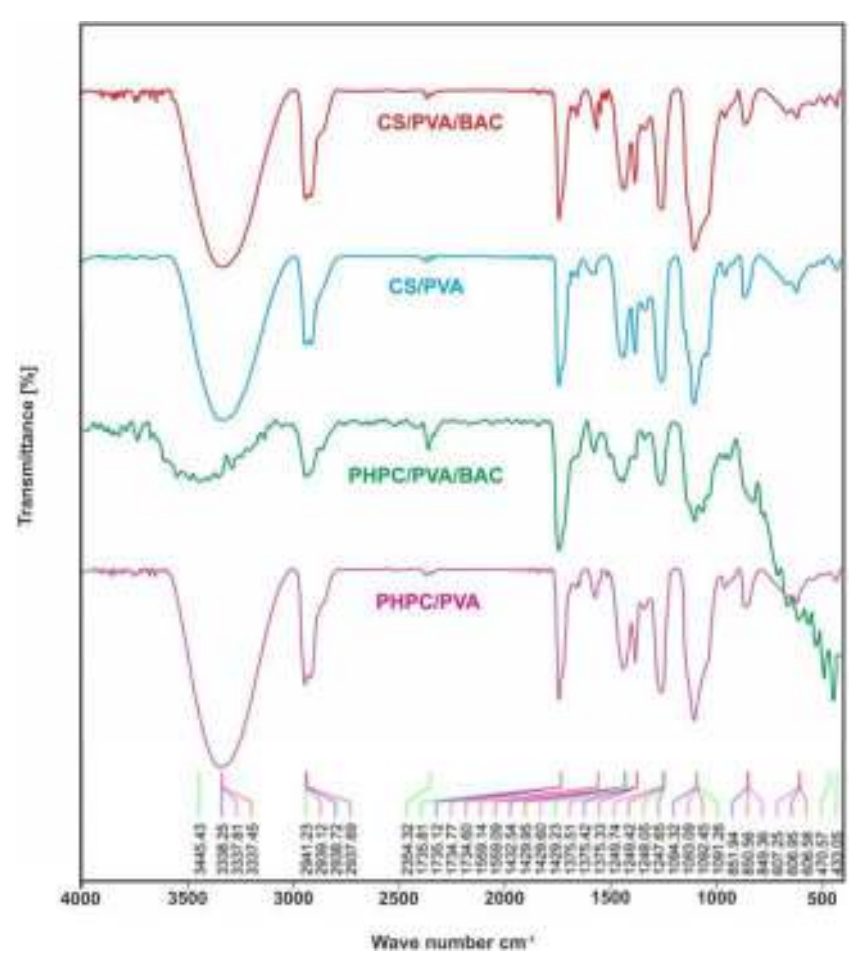


Fig. 2. FT-IR spectra of CS/PVA, PHPC/PVA, CS/PVA/BAC, and PHPC/PVA/BAC skin scaffolds.

3.2.8. DSC property

The Differential Scanning Calorimetry (DSC) thermograms were used to analyze the thermal behaviors of various nano scaffolds including CS/PVA, CS/PVA/BAC, PHPC/PVA, and PHPC/PVA/BAC, as well as individual compounds CS and PVA (Figs. 3 and S4). When BAC was in its crystalline form, a single depression was observed at its melting point, while no melting peak was observed when the drug was amorphous. The DSC thermograms of pure BAC exhibited an endothermic peak near its melting point temperature range and an exothermic peak related to flavonoid oxidation (Tm baicalin = 212.9 °C), which has been reported in the literature [99,100]. Additionally, it displayed a wide absorption peak at 120.3°C, attributed to the dehydration of baicalin [99]. The absence of phase transitions indicated that BAC in CS/PVA/BAC and PHPC/PVA/BAC was molecularly dispersed and might have been in an amorphous form, allowing for easier dissolution [100]. The disappearance of the melting point peaks of baicalin suggested the success of the inclusion complexation, concealing the crystal characteristics of the drug [99]. According to previous reports, PVA typically melts within a certain temperature range, during which the degradation of PVA begins [101]. Therefore, the melting of PVA was not detected in this study. The dissolution rate of BAC is influenced by the surface area and the degree of crystallinity of the compound. The amorphous forms of flavonoids offer improved solubility and compatibility, but their instability presents challenges due to their inclination to transform back into a crystalline phase [102]. Furthermore, the cross-linked structure of flavonoids was observed to enhance their thermal properties by limiting heat and oxygen access to BAC particles, thereby retarding thermal decomposition and oxidation processes [103].

3.2.9. Drug release

The drug concentration (BAC) in the electrospinning solution was standardized at 100 μM based on the survival rate results of MDF cells (Fig. S5). The drug content per cm² of CS/PVA/BAC and PHPC/PVA/BAC scaffolds was found to be 0.21 \pm 0.03 mg and 0.23 \pm 0.02 mg, respectively. The drug amount in each scaffold ranged between 98 and 102% of the nominal amount, indicating uniformity in drug content. BAC molecules were distributed throughout the polymer matrix of CS/PVA/BAC and PHPC/PVA/BAC scaffolds as there was no membrane acting as a diffusion barrier in this matrix-type system. This system exhibited a high initial release rate, followed by a decreased release rate associated with the diffusion distance of the drug molecule within the solution medium [104]. After 5 hours, the high-release phase resulted in the release of 18% and 24% of BAC through the CS/PVA/BAC and

PHPC/PVA/BAC scaffolds, respectively (Fig. 4). During the sustained release phase of 96 hours, the release rate further increased, resulting in the release of 67.3% and 76.8% of BAC from the CS/PVA/BAC and PHPC/PVA/BAC scaffolds, respectively (P<0.05). This is attributed to the hydrophilic property of PHPC and its rapid swelling after long-term In diffusion-mediated controlled release system, post-solubilization the diffusion kinetics of a drug molecule is the limiting factor. The drug-containing core is enveloped by a polymeric nanofibrous membrane, creating a reservoir system. As the drug concentration decreases between the two sides of the scaffolds, the release rate at the end of the test also decreases [104]. Flavonoids like BAC face challenges in reaching their intended targets in effective doses due to their poor solubility and bioavailability in pharmacokinetic studies. However, electrospun nanofiber-based films can serve as smart drug carriers to improve BAC dispersion, solubility, drug wettability, stability, and performance both in vitro and in vivo [43,81,105].

While baicalin displayed a slow release pattern through scaffolds with different hydrophilic and lipophilic properties in this study, a previous report demonstrated that an injectable BAC/Pluronic® F-127 hydrogel exhibited a rapid release, with over 70% of the baicalin being released within the first 8 hours, followed by a gradual release over the next 16 hours [42]. In another studies, the CS/dioleyl phosphatidyl ethanolamine/baicalein nanohydrogel containing 8.6% drug released approximately 65% of baicalein within 24 hours [106]. Additionally, baicalin-loaded core-shell structure scaffolds, composed of size-stable poly-caprolactone (PCL) and Poly (lactic-co-glycolic acid) (PLGA), released 73.2% of the loaded baicalin after 28 days. The hydrophobic

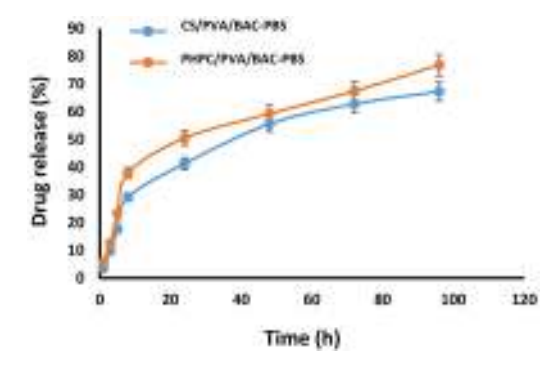


Fig. 4. Release profiles of BAC from CS/PVA/BAC, and PHPC/PVA/BAC skin scaffolds in PBS at pH 7.4 for 96 h. The data are expressed as mean \pm SD from three independent experiments.

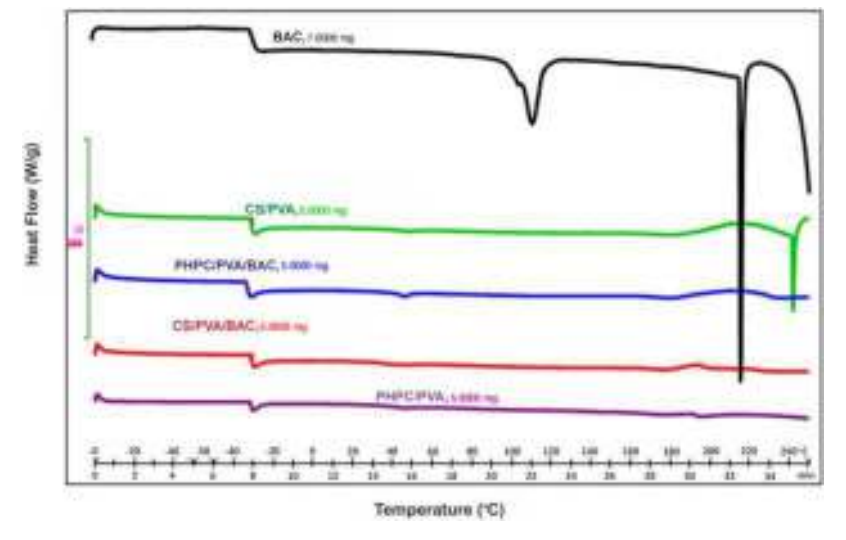


Fig. 3. DSC patterns of BAC, CS/PVA, CS/PVA/BAC, PHPC/PVA, and PHPC/PVA/BAC skin scaffolds.

properties and core-shell structure of the PCL/PLGA scaffolds acted as a physical barrier against baicalin diffusion [81]. In contrast, CS/PVA and PHPC/PVA scaffolds exhibited faster release due to their hydrophilic nature, fast water infiltration, and low physical barrier against baicalin diffusion. On another side, targeted drug delivery techniques have improved the bioactivity of therapeutics and the controlled release of drugs. In this context, the pH-responsive drug release capability of a baicalein-encapsulated drug delivery system (DDS) with a zeolite imidazole framework-8 (BA@ZIF-8) as a treatment carrier showed a cumulative drug release of up to 65.8% at an acidic pH \sim 5 and 52.46% at a pH \sim 6. This suggests that the decomposition or cleavage of the nanocomposite wound closure material may depend on their drug-loading capacity and the pH-responsive drug release mechanism [107].

Since wound dressings are typically applied for several days, a slow and sustained release pattern could be an ideal model for continuous drug delivery. To investigate this, the release kinetics of baicalin was analyzed using various mathematical models [108]. The suitability of the delivery system was evaluated based on the regression coefficient (R^2) values close to 1. In this study, (R^2) values were calculated for various models including first-order (($R^2 = 995$, and 989), zero-order $(R^2 = 916 \text{ and } 926)$, and Higuchi's model $(R^2 = 954 \text{ and } 942)$ in CS/PVA/BAC and PHPC/PVA/BAC scaffolds, respectively. The results confirmed that baicalin adhered to the first-order kinetic model with strong linearity for both scaffolds, consistent with a prior study on baicalin/F127 hydrogel [42]. The release mechanism of BAC may involve polymer matrix swelling and drug diffusion, suggesting that baicalin follows a first-order kinetic model where the release is controlled by drug dosage and diffusion through the nanofiber matrix. Desorption from the surface of the nanofibrous mat is proposed as the primary mechanism for baicalin release and independent from the biodegradation of the nano scaffold, as reported in previous studies [42,105,109, 110]. To address the limitations of using a single material as a carrier, a combination of two or more carrier materials with distinct hydrophobic, hydrophilic, and coating properties is commonly used to enhance pharmaceutical formulations and improve the solubility of active/natural compounds [111]. Baicalin molecules were probably bound to the primary hydrophobic binding sites of Pr and HyP within the PHPC from the nanofiber mats. Hydrophobic interactions and strong hydrogen bonding may have occurred, involving the -OH groups of baicalin interacting with the oxygen and nitrogen of PHPC. Additionally, the benzene ring may have been involved in hydrophobic interactions with amino acids of PHPC and formed non-covalent π -stacking interactions, indicating the important role of baicalin in regulating the cross-interaction process [112,113]

Although baicalin capsules were approved for adjuvant therapy of hepatitis by the State Food and Drug Administration of China in 2005 [114] when applied topically, baicalin still presents limitations including rapid hydrolysis to its aglycone baicalein by the β -glucuronidase enzyme during the wound-healing phase [114,115] extensive binding to human plasma proteins (86–92%) [116] a short elimination half-life (6.36 \pm 5.85 h) [91] poor permeability [46,89] and reduced cell viability at high doses (\geq 200 μ g/ml) [117]. These drawbacks have hindered its practical application in drug production, highlighting the importance of finding ways to enhance its bioavailability through solubilization. The current wound dressing effectively releases baicalin in a controlled and sustained manner over a prolonged period, eliminating the requirement for frequent dressing changes.

3.3. Biological properties of the skin scaffolds

3.3.1. Drug dosage

The results presented in Fig. S5 demonstrate that different levels of BAC (ranging from 25-125 μ M) have varied impacts on MDF cell proliferation. At lower concentrations, BAC did not significantly affect MDF cell viability, whereas higher concentrations led to decreased cell

viability. Even when administered at a concentration of 100 μ M, cell viability remained at approximately 85%. This suggests that BAC could potentially support wound healing as it does not emit harmful substances in dressing materials. However, scientific evidence indicates that BAC possesses toxicity potential in a cell-specific and dose-dependent manner [117,118]

3.3.2. Morphology of cell-hybrid scaffolds

The SEM images shown in Fig. 5 reveal that both the CS/PVA/BAC and PHPC/PVA/BAC skin scaffolds exhibit a porous and fibrous structure, creating a suitable surface for MDF cells to adhere and spread along the surface of the nanofibrous mats. The MDF cells not only grew and covered the edges of the biomaterials but also integrated into the scaffold pieces.

Cells seeded on both sides of the nanofiber scaffolds facilitated the bonding of adjacent membranes through the secretion of ECM. However, it is important to note that the tightly packed electrospun nanofiber mats may have limitations due to their 2D structures, which restrict cell penetration and growth within the nanofiber matrix [119]. Therefore, it is crucial to develop a novel approach for creating electrospun scaffolds that possess a stable 3D structure, while also displaying nanofibrous morphologies and deep interconnected pores. This will provide an additional direction for cell-cell interactions, cell migration, and cell morphogenesis, all of which are vital in regulating the cell cycle and tissue functions [119].

3.3.3. Cytotoxicity and cell viability

Engineered materials with non-immunogenic, non-toxic, flexible, and degradable properties are excellent for creating scaffolds that mimic a natural microenvironment for cells. These cell-hybrid scaffolds can support interactions between nano-biomaterials, stem cells, and the ECM, providing a surface for cell adhesion and proliferation, as well as a structure for tissue regeneration [120]. As shown in Fig. 6, the CS/PVA and PHPC/PVA nanofiber scaffolds showed great cytocompatibility and positively influenced the growth of skin fibroblast cells. This is likely due to the presence of proline and hydroxyproline, which provide a biomimetic microarchitecture for cell adhesion and growth. The MTT assay results also revealed that the PHPC/PVA scaffolds were significantly better at promoting cell proliferation compared to the CS/PVA scaffolds (P<0.05). The pH range of burned skin upon admission was found to be 6-9.5 [121]. Chitosan, with a pKa of 6.5, can solubilize in acidic pH due to the protonation of free amino groups leading to a higher surface charge and positive zeta potential. These pH-sensitive properties of chitosan allow for better interaction with cells, enhanced cellular uptake, and selective drug release in specific microenvironments in and around cells [122]. Modifications in PHPC-based scaffolds resulted in decreased surface cationic density, and lower ionic interaction with the negatively charged cell membrane, making them less toxic and more suitable for cell attachment compared to native CS [38,98].

Fig. 7 illustrates the presence of viable cells in nanofiber scaffolds using various staining methods such as EB/AO and DAPI. Through fluorescence staining, changes in the color of the nuclear chromatin indicated DNA condensation, nuclei fragmentation, and chromatin degradation, distinguishing between living, dying, and dead cells [123, 124]. This staining approach allowed for the differentiation of apoptotic MDF fibroblast cells with damaged membranes (red and light blue cells) from the intact cell membrane of alive cells (green and blue cells). The staining methods and MTT test confirmed the cytocompatibility and biodegradability of PHPC/PVA and PHPC/PVA/BAC nanofibrous scaffolds, making them a well-suited matrix for promoting cellular skin fibroblast response, deposition, and proliferation in regenerative medicine applications [81,98].

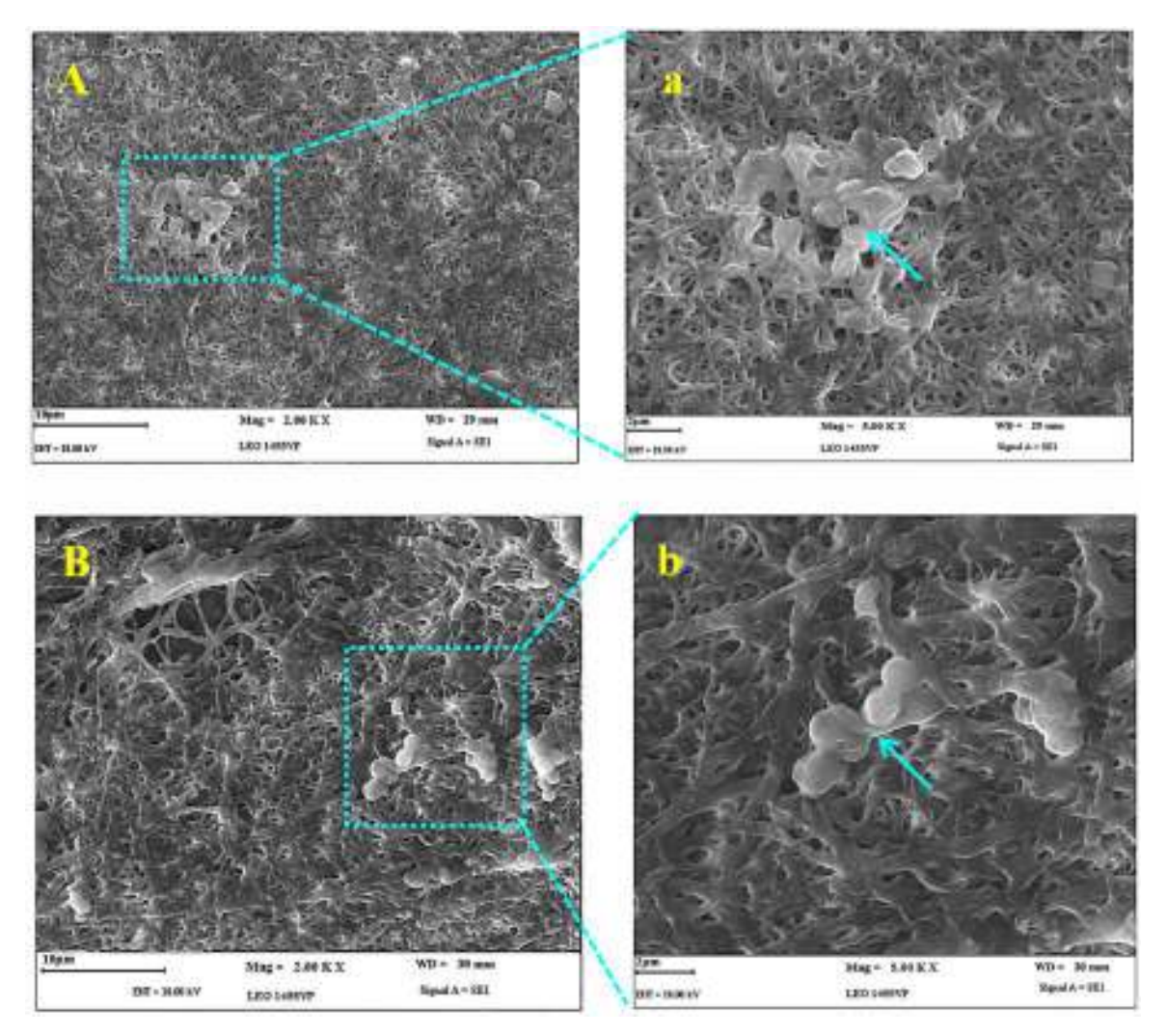


Fig. 5. Scanning electron micrographs showing the morphology of cell-hybrid scaffolds 24 h after fibroblast seeding over PHPC/PVA/BAC (A), and CS/PVA/BAC (B), skin scaffolds. The MDF cells are indicated with blue arrows, shown at both low magnification (A, B) and high magnification (a, b).

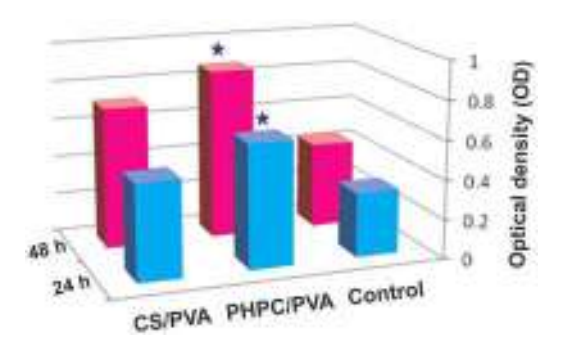


Fig. 6. Cell-loaded in CS/PVA, PHPC/PVA, and well plate without nanofiber (control) survival in MTT assay at 24 and 48 h. Data are presented as mean \pm SD (n=3); *P < 0.05.

3.4. In vivo study

3.4.1. Wound healing (macroscopic views)

During the wound-repairing process, particularly the inflammation phase, the cytoprotective activity and antioxidant capacity of baicalin play a significant role [41,42]. As shown in Fig. 8, the change in wound area after 7 and 14 days of treatment with different nanofiber scaffolds is illustrated, while Fig. 9 presents the percentage of total wound closure

and the relative contributions of contraction and re-epithelialization after 3, 7, and 14 days post-injury. The results indicate that within the control groups, 60% of the wounds had healed after 14 days, demonstrating a self-healing effect. In the case of CS and PHPC blank and BAC-loaded CS/PHPC nanofibers, no significant difference was observed compared to the control group after 3 days. However, a significantly accelerated wound healing (P=0.041) was evident after 7 days of treatment with PHPC-based scaffolds. This enhanced wound healing may be attributed to the regulatory role of proline and hydroxyproline metabolism in collagen biosynthesis and cellular metabolism (particularly the synthesis of arginine, polyamines, and glutamate through pyrroline-5-carboxylate, which contributes to collagen rebuilding) [38, 125,126]. It was observed that almost complete wound closure was achieved after 14 days of treatment for both CS and PHPC blank and BAC-loaded CS/PHPC nanofiber scaffolds. However, PHPC-based scaffold groups exhibited significantly lower unclosed wound areas than the control group (P<0.05). Moreover, the addition of mouse fibroblast cells enhanced the wound healing effect of both CS/PVA/BAC/MDF and PHPC/PVA/BAC/MDF scaffolds compared with controls (P<0.05) [127]. Notably, the findings suggest that BAC-loaded PHPC-based nanofibers have superior wound repair properties compared to CS-based scaffold counterparts [98] which may be attributed to the amplified antioxidant activity of BAC through its interactions with MDF cells, although the specific mechanism remains unclear. Plausibly, the accumulation and activation of play a key role in the formation of

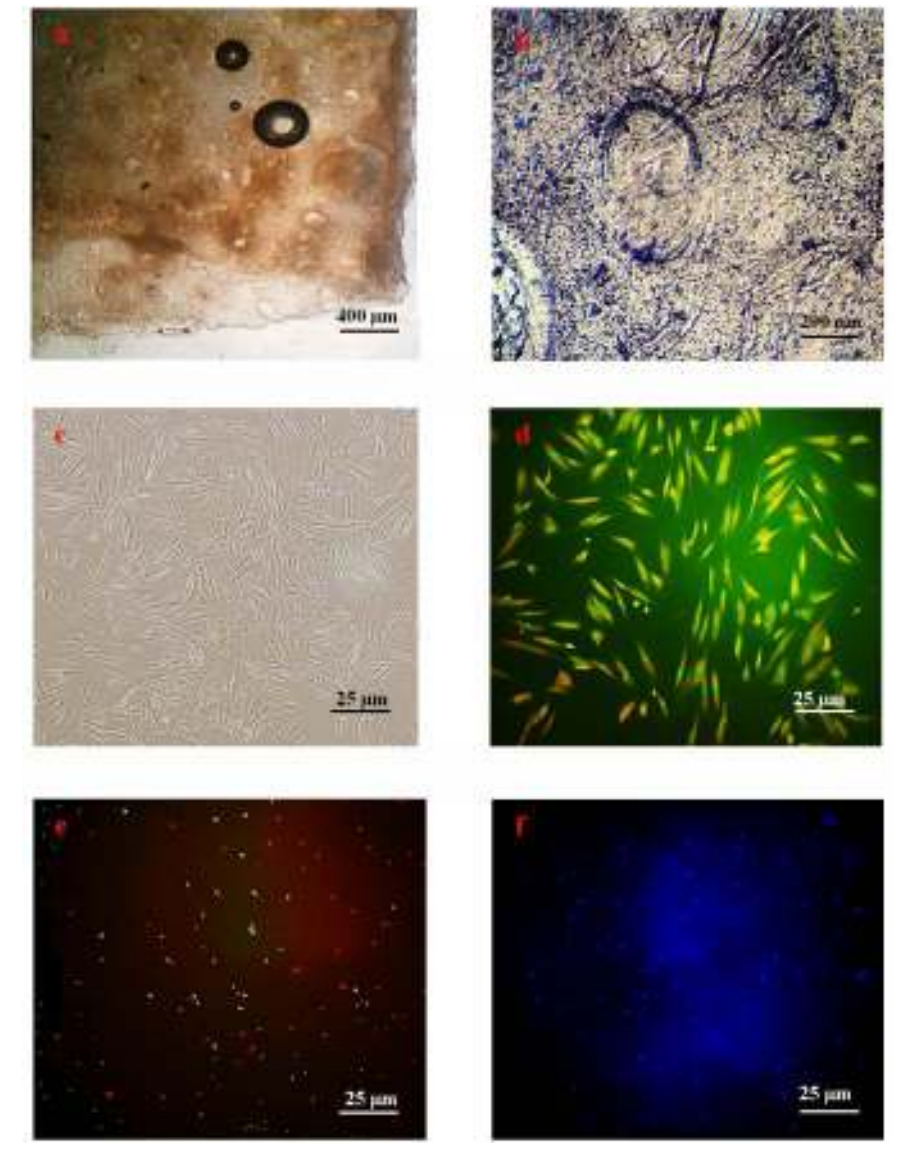


Fig. 7. The PHPC/PVA scaffolds in both 3D (a) and 2D (b) views, MDF cells characteristics 24 hours before loading on nanofiber mats (c), and fluorescence microscopy images of cell viability on the PHPC/PVA nanofibrous scaffolds (d). Dual EB/AO staining of loaded cells after 24 hours of seeding on scaffolds (e), showing the live (AO, green) and dead (EB, red) cells. DAPI staining showing non-induction of apoptosis in MDF cells on the PHPC/PVA/BAC (f).

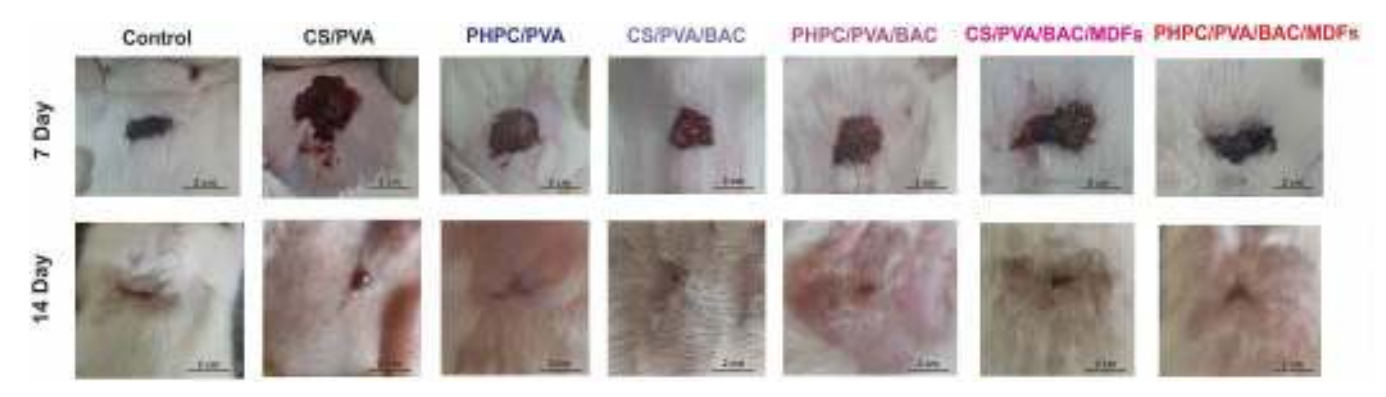


Fig. 8. Macroscopic view of wound changes on days 7 and 14 in the control group and treatment skin scaffold groups, including CS/PVA, PHPC/PVA, CS/PVA/BAC, PHPC/PVA/BAC, CS/PVA/BAC/MDFs, and PHPC/PVA/BAC/MDFs.

granulation tissue and wound contraction, which accelerates the healing process [127]. Apart from releasing soluble mediators through ECM remodeling, fibroblasts also secrete and activate bioactive factors such

as $TGF\beta$ that can impact tissue repair, and release lysyl oxidase, which assists in ECM degradation via matrix metalloproteinases (MMPs), thereby facilitating cell invasion into injured tissues and influencing

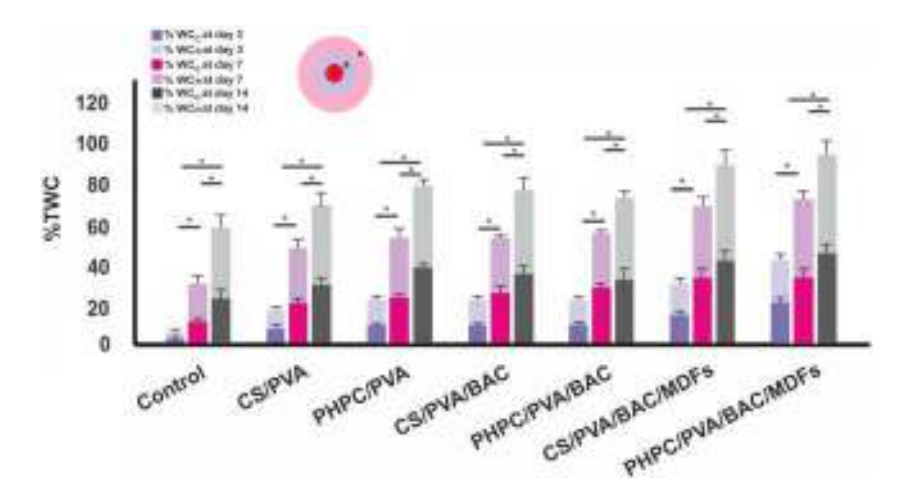


Fig. 9. The percentage of total wound closure (TWC) was determined by assessing the wound closure attributable to re-epithelialization (WC_R) and wound closure attributable to contraction (WC_C) at different time points. To calculate this, the area of the remaining wound was divided into the original wound (A), newly reepithelialized skin (B), and wound contraction (C). The percentages of WC_R and WC_C were measured as ([B-C]/B \times 100) and ([A-B]/A \times 100), respectively. The data are shown as mean \pm SD (n=5); *P < 0.05, ns, not significant.

tissue rigidity and porosity [127,128]. In this way, the bioactive molecules released by fibroblasts act in paracrine ways to influence the functions other cells cell involved in immune regulation. Additionally, fibroblasts secrete proinflammatory cytokines such as tumor necrosis factor- α , interleukins, and C-C and C-X-C chemokines, which attract neutrophils, monocytes, and macrophages to the affected wound sites [127–130].

In terms of quantifying wound healing, the percentage of wound closure attributed to contraction was generally less than $\sim\!66\%$ and ~73% in the blank and BAC-loaded CS/PHPC nanofiber scaffolds, respectively, whereas the percentage levels of WCR was greater than WC_C at each time point analyzed (Fig. 9) [131]. These findings indicate that a significant part of closure in murine excisional wounds enhances re-epithelialization for all groups, with the highest % WCR rate of 92 \pm 1.3% and 87 \pm 1.1% observed for PHPC/PVA/BAC/MDF and CS/PVA/BAC/MDF on day 14, respectively (P<0.05) (Fig. 9). However, although the contraction continued to increase from day 7 to 14 for all groups, on day 14, the final observation time, the apparent contribution of contraction to TWC increased relative to that of re-epithelialization. particularly in MDF and BAC-loaded CS/PHPC nanofiber scaffolds, which exhibited the highest % WC_C rate of 43 \pm 1.6% and 41 \pm 1.2% on day 14, respectively (P<0.05) (Fig. 9). The results suggest that while murine excisional wounds do demonstrate contraction, the level of contraction is limited until complete epithelial closure is achieved [131]. Subsequently, the wound continues to contract upon closure, giving the impression of predominant closure through contraction. These results align with previously reported data indicating a contribution of 50% \le by re-epithelialization during the phase of wound closure using potential therapeutic electrospun nanofiber mats [132]. In comparison with other BAC-loaded advanced materials, previous studies have shown that baicalin-containing hydrogels and nanohydrogels have demonstrated accelerated wound healing and inhibition of specific inflammatory markers. For example, baicalin/F127 hydrogel resulted in almost complete wound closure after 15 days of treatment [42] while baicalin-coordinated borate ions/bacterial cellulose (Bai-B/BC) composite hydrogel significantly accelerated the healing process of chronic wounds, promoting uniform and orderly collagen deposition after 17 days of treatment [133]. Additionally, a gellan-cholesterol nanohydrogel containing baicalin accelerated wound healing in 12-O-tetradecanoylphorbol 13-acetate (TPA)-injured skin mice after 3 days [134]. Baicalein-functionalized collagen scaffolds (BFCSs) have also shown promise in inducing tissue regeneration and directing neuronal differentiation to enhance spinal cord injury repair [135]. Nevertheless, the current research suggests that biodegradable fibroblasts loaded

PHPC-originated nanofibers could be a promising candidate for cell-based therapy due to their potential to enhance the proliferation of dermal and epidermal cells, and promote the formation of granulation and epithelial tissues [136] regardless of the effective role of BAC in wound healing.

3.4.2. Histocompatibility (microscopic views)

All dermal wounds heal through three primary mechanisms: contraction, connective tissue matrix deposition, and epithelialization [137]. The histopathological features of wounds in various groups are depicted in Fig. 10A. Following 7 days of treatment, the control group exhibited thick scabs with numerous inflammatory cells and cellular infiltration, and by day 14, it showed the lowest keratinocyte proliferation compared to the treated groups. The maturation phase was incomplete by day 14, and the fresh wound dried much quicker than the treatment groups with scaffolds, as thick collagen fiber bundles were not observed. In the CS/PVA and PHPC/PVA groups, the site of inflammatory exudates was evident, along with the infiltration of inflammatory cells, particularly neutrophils (Fig. 10A). Abundant fibroblast cells and blood vessels comprised the organization of collagen fibers and the granulation tissue on the floor and sides of the wound. In the case of the blank PHPC/PVA nanofiber, the proliferation phase commenced on day 3 and persisted until day 14, with the maturation phase initiating on day 14, as collagen fibers were detected in the wound. The incorporation of phenolic flavonoid antioxidant substances like BAC in PHPC/PVA/BAC nanofibers expedited the inflammation and maturation phases, leading to the presence of more keratinocytes, and inflammatory cells such as macrophages, and neutrophils, as well as collagen fibers and ordered connective tissue [41]. The proliferation of fibroblast cells within the BAC-loaded PHPC scaffolds enhanced the accelerating effect of BAC on wound healing, generating and relocating numerous keratinocyte cells to the wound. The formation of collagen fiber was also evident 3 days post-treatment and continued through day 14. Similar outcomes were observed in the case of CS/PVA/BAC/MDF, however, PHPC/PVA/-BAC/MDF proved to be a superior scaffold for keratinocyte proliferation and collagen fiber appearance compared to its CS-based counterpart, suggesting a more pronounced impact on wound healing [41].

Re-epithelialization (epithelial regeneration) is crucial for effectively closing a wound. Within a day of the injury, basal cells from the lower layer of the skin near the wound start multiplying and moving toward the damaged area until the skin has returned to its normal thickness [138]. In this line, on the 7th day, the treated BAC-based groups showed significantly improved epithelialization and neovascularization compared to the control group, as well as groups treated with blank

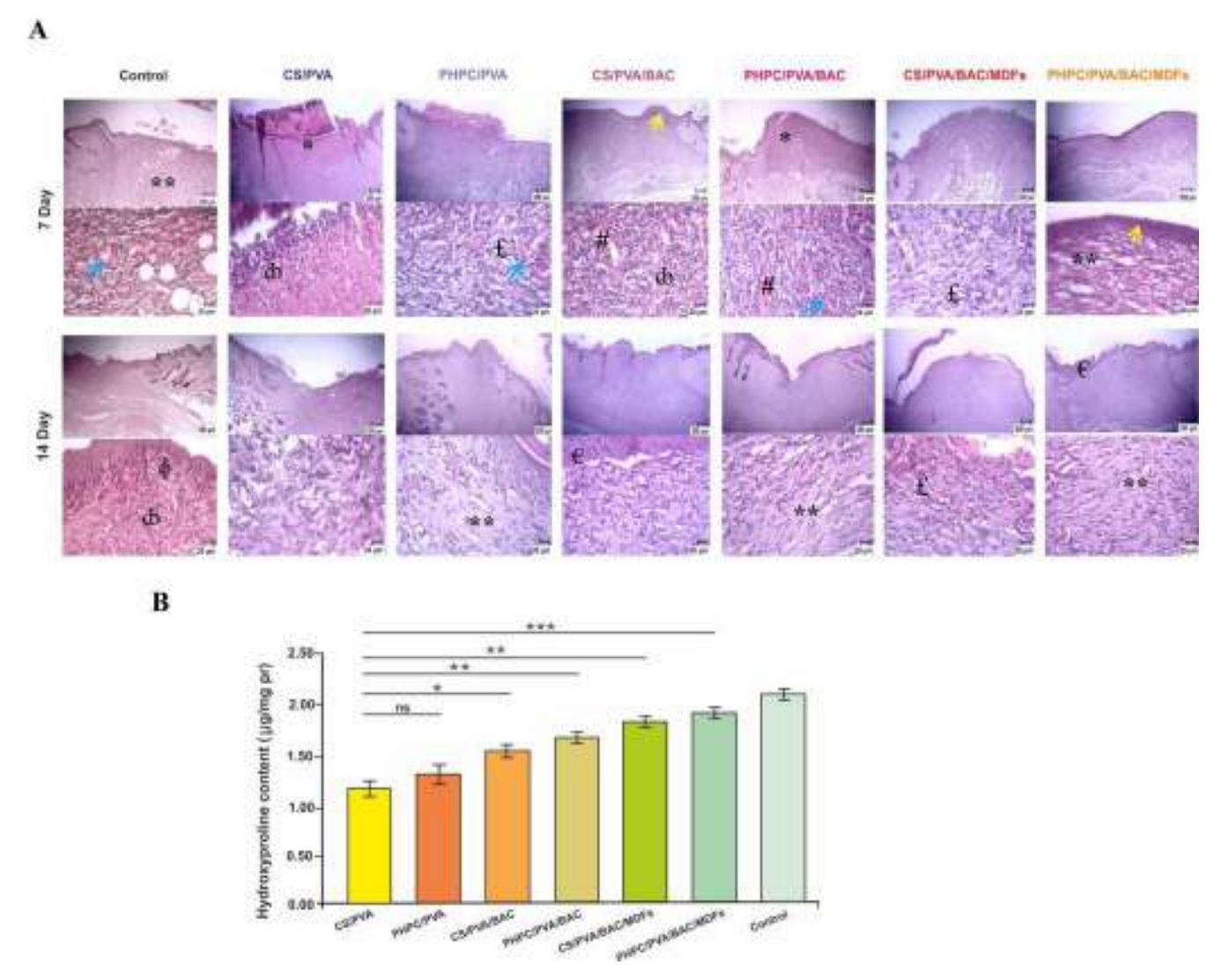
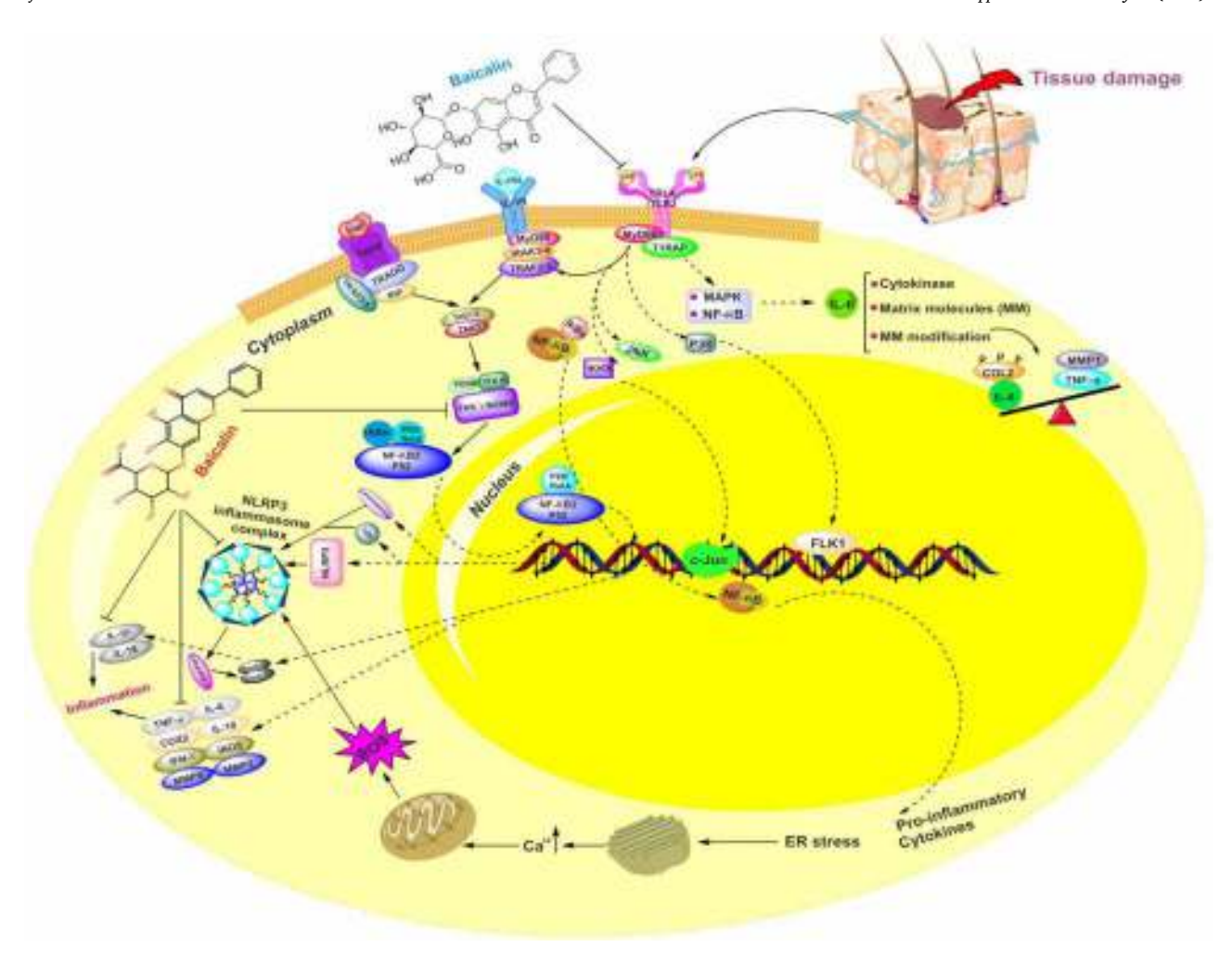


Fig. 10. (A) Microscopic view (H&E staining) was conducted to assess the wound healing effects of skin scaffolds at 7 and 14 days in various groups including the control group, CS/PVA, PHPC/PVA, CS/PVA/BAC, PHPC/PVA/BAC, CS/PVA/BAC/MDFs, and PHPC/PVA/BAC/MDFs groups. £ indicates fibroblast, ϕ indicates keratinocytes migration, ** indicates collagen, *indicates granulation tissues, θ indicates epithelial tissues, # indicates the blood vessel, θ indicates inflammatory cell infiltration, yellow arrow indicates the epithelialization, and blue arrow indicates the neovascularization. (B) Hydroxyproline content (µg/mg protein) for all studied group after 14 days. Error bars show the means θ SD (θ = 5), *P < 0.05, **P < 0.01, ***P < 0.001.

CS/PHPC-based scaffolds. Histopathological analysis confirmed that the BAC-loaded tissue-engineered nanofibrous scaffolds of CS/PHPC and CS/PHPC-MDF demonstrated increased collagen deposition, and epidermal and granulation tissue thickness, nearly completed epithelial regeneration with normal keratinization and remodeling of connective tissue, and enhanced angiogenesis, all contributing to the observed improved wound healing effects (Fig. 10A) [41,128]. To support this, baicalin has been shown to reduce the inflammatory response by recruiting M2 macrophages (pro-healing) to the implantation site by modulating the polarization of M1 macrophages towards the M2 phenotype and downregulating the expression of macrophage migration inhibitors monocyte chemo-attractant protein (MCP)-1 and macrophage inflammatory protein (MIP)-3a [49,50]. Baicalin also reduces the time of healing and contraction of the wound while increasing the rate of epithelialization possibly mediated by stimulating angiogenesis-related gene expression through the vascular endothelial growth factor (VEGF) and MMP pathways [41,49]. Aside from our results relying on baicalin's effectiveness in promoting keratinocyte migration and fibroblast proliferation, topical application of baicalin on reconstituted murine hair follicles has demonstrated an increase in the development of terminal hair by activating Wnt/β-catenin signaling and dermal papillar cells [41,51]. This indicates that baicalin impacts various processes at the wound site, including keratinocyte and fibroblast interaction, synthesis and breakdown of ECM proteins, fibroblast chemotaxis, and regulation of the immune response [41,51,52,128]. The baicalin-loaded PHPC/CS has been found to enhance immune regulation and prevent inflammatory infiltration, accelerating the maturation phases of cells involved in dermal wound healing. In a related in vivo study, it was observed that baicalin downregulated the expression of inflammatory cytokines IL-1β, IL-6, and TNF-α by regulating autophagy via Akt/mTOR and the ROS-mediated p38 MAPK signaling pathway, thereby improving paracellular permeability [47,53–56]. This flavonoid also led to reduce the expression levels of apoptotic genes Bcl-2 and caspase-9 in a dose-dependent fashion [55] suppress the IKB kinase complex (IKK)/IKB/NF-κB signaling pathway [55] and block TLR-4/NF-κB-p65/IL-6 signaling pathway [57] highlighting its anti-inflammatory role in PHPC/PVA/BAC/MDF nanofibrous scaffolds toward the faster wound healing potential (Scheme 2). However, more studies are needed to explore the clinical application of baicalin, as well as its synergistic or antagonistic effects in combination with other drugs.



Scheme 2. Schematic diagram of baicalin-based inhibited inflammation-related signaling pathways, whereas inflammation results are produced by tissue damage [41,47,49–57].

Additionally, further research on the long-term toxicity, pharmacokinetics, and pharmacodynamics of these phytomedicines is necessary to maximize their efficacy in various skin diseases.

3.4.3. Collagen deposition

The process of wound healing involves the remodeling and synthesis of collagen, which is a crucial and lengthy final step. Proline and its derivative, hydroxyproline, are the backbone of collagen synthesis, making up \sim 23% of the amino acid content in collagen, and play a key role in reducing scar thickness and strengthening the skin around the wound [139]. Excessive availability of hydroxyproline at the wound site can up-regulate collagen expression, particularly type I collagen, as well as HIF- 1α expression [139,140]. Thus, the rendering assays of this amino acid in granulation tissue was used as a collagen turnover index. The data presented in Fig. 10B indicates a significant increase in hydroxyproline deposition in rat skin tissue treated with PHPC/PVA/BAC/MDF and CS/PVA/BAC/MDF on day 14 post-incision (P<0.05). Notably, the PHPC/PVA/BAC/MDF group exhibited higher hydroxyproline content compared to all other groups (P<0.05), reaching an equivalent level to the sham control. However, there was no observable difference in collagen deposition between the blank scaffolds of CS/PVA and PHPC/PVA at the end of the experiment. Of note, the BAC-loaded PHPC-based blank scaffolds demonstrated a noticeable increase in hydroxyproline deposition compared to other CS-based blank/control groups (P<0.05) (Fig. 10B). Additionally, the concomitant use of the drug (BAC) with PHPC/PVA scaffolds led to the relatively high amount of hydroxyproline, which was found to be crucial in stimulating messages for collagen synthesis, inducing cell proliferation, and modulating collagen metabolism and deposition at the wound site. In contrast to baicalin stimulates collagen synthesis [41,42,81,98] some evidence suggests that baicalein has shown potential in alleviating TGF β1-induced type I collagen production in lung fibroblast cells by downregulating connective tissue growth factor (CTGF) [128]. However, despite the identified regulation of collagen biosynthesis at the level of insulin-like growth factor-I receptor (IGF-IR), β1-integrin receptor, and NF-kB signaling as a mechanism for drug-dependent regulation, recent data has provided evidence that the process of proline-dependent regulation of collagen metabolism can significantly increase collagen biosynthesis in cultured cells, especially in a glutamine-free medium [125]. Overall, this research provides valuable insights into the relationship between baicalin-based dressing biomaterials and collagen production, offering a promising strategy for burn wound healing.

4. Conclusions

In the present study, a new approach using electrospinning was developed to create innovative nanoscaffolds for third-degree burn wound recovery in a rat model by using a combination of Pr and HyP functionalized CS derivative (PHPC), PVA, natural flavonoid of baicalin (as drug), and MDF cells. The PHPC/PVA/BAC/MDF nanoscaffolds depicted a porous structure with favorable physico-chemical characteristics, moisture absorption ability, and cytocompatibility properties. The results indicated that these nano-composites provided improved

therapeutic benefits for managing burn wounds compared to other CSbased composite and blank PHPC/CS-based counterparts. Our findings suggest that these rendered encouraging cellularized dressing of collagenous amino acid-based nanofibrous scaffolds with BAC-loaded bioactivities could assist wound angiogenesis, re-epithelialization, contraction enhancement, and reduce wound healing time, leading to complete treatment within just 14 days.

Funding sources

The study was funded by Ahvaz Jundishapur University of Medical Sciences (Grant No: N-0103).

CRediT authorship contribution statement

Azam Sharifi: Visualization, Methodology, Investigation. Sakineh Mashjoor: Writing - review & editing, Writing - original draft, Visualization, Validation, Software, Project administration, Methodology, Investigation, Formal analysis, Data curation, Conceptualization. Behzad Sharif Makhmalzadeh: Writing - review & editing, Writing original draft, Visualization, Validation, Supervision, Software, Resources, Project administration, Funding acquisition, Data curation, Conceptualization. Layasadat Khorsandi: Formal analysis, Data curation. Mohammad Reza Shushizadeh: Methodology, Formal analysis, Data curation.

Declaration of competing interest

The authors declare that they have no known competing financial interests or personal relationships that could have appeared to influence the work reported in this paper.

Acknowledgments

This study was Pharm D thesis of Azam Sharifi from School of Pharmacy, Ahvaz Jundishapur University of Medical Sciences, Iran.

Supplementary materials

Supplementary material associated with this article can be found, in the online version, at doi:10.1016/j.apmt.2024.102519.

Data availability

Data will be made available on request.

References

- [1] P. Baker, C. Huang, R. Radi, S.B. Moll, E. Jules, J.L. Arbiser, Skin barrier function: the interplay of physical, chemical, and immunologic properties, Cells 12 (2023)
- W. Żwierełło, K. Piorun, M. Skórka-Majewicz, a A Maruszewsk, J. Antoniewski, I. Gutowska, Burns: classification, pathophysiology, and treatment: a review, Int. J. Mol. Sci. 24 (4) (2023) 3749.
- [3] L. Si, X. Guo, H. Bera, Y. Chen, F. Xiu, P. Liu, C. Zhao, Y.F. Abbasi, X. Tang, V. Foderà, D. Cun, M. Yang, Unleashing the healing potential: exploring nextgeneration regenerative protein nanoscaffolds for burn wound recovery, Asian J. Pharm. Sci. 18 (6) (2023) 100856.
- [4] H.N. Wilkinson, M.J. Hardman, Wound healing: cellular mechanisms and pathological outcomes, Open. Biol. 10 (9) (2020) 200223.
 [5] A. Cioce, A. Cavani, C. Cattani, F. Scopelliti, Role of the skin immune system in
- wound healing, Cells 13 (2024) 624.
- [6] F. Cialdai, C. Risaliti, M. Monici, Role of fibroblasts in wound healing and tissue remodeling on earth and in space, Front. Bioeng. Biotechnol. 10 (2022) 958381.
- [7] R.B. Diller, A.J. Tabor, The role of the extracellular matrix (ECM) in wound healing: a review, Biomimetics 7 (3) (2022) 87 (Basel).
- [8] R.E. Atwood, M.J. Bradley, E.A. Elster, Use of negative pressure wound therapy on conflict-related wounds, Lancet Glob. Health 8 (3) (2020) 319-320.
- C. Yang, C. Yang, Y. Chen, J. Liu, Z. Liu, H.J. Chen, The trends in wound management: sensing, therapeutic treatment, and "theranostics", J. Sci. Adv. Mater. Dev. 8 (4) (2023) 100619.

- [10] V. Popescu, V. Cauni, M.S. Petrutescu, M.M. Rustin, R. Bocai, C.R. Turculet, H. Doran, T. Patrascu, A.M. Lazar, D. Cretoiu, V.N. Varlas, B. Mastalier, Chronic wound management: from gauze to homologous cellular matrix, Biomedicines 11 (9) (2023) 2457.
- [11] M. Afshar, A. Rezaei, S. Eghbali, S. Nasirizadeh, E. Alemzadeh, E. Alemzadeh, M. Shadi, M. Sedighi, Nanomaterial strategies in wound healing: a comprehensive review of nanoparticles, nanofibres and nanosheets, Int. Wound J. 21 (7) (2024) e14953
- [12] Y.C. Lin, C.Y. Lee, J.R. Jones, W.C. Liu, N.J. Cho, C.C. Hu, R.J. Chung, Sustained Antibiotic release from biodegradable gelatin-silica hybrid for orthopedic infections, Adv. Funct. Mater. (2024) 2409491, https://doi.org/10.10 adfm.202409491.
- [13] B. Borban, M.B. Gohain, D. Yadav, S. Karki, P.G. Ingole, Nano-electrospun membranes; green solutions for diverse industrial needs, J. Hazard, Mater, Adv. 12 (2023) 100373.
- Z. Jiang, Z. Zheng, S. Yu, Y. Gao, J. Ma, L. Huang, L. Yang, Nanofiber scaffolds as drug delivery systems promoting wound healing, Pharmaceutics 15 (7) (2023)
- G.G. Flores-Rojas, B. Gómez-Lazaro, F. López-Saucedo, R. Vera-Graziano, E. Bucio, E. Mendizábal, Electrospun scaffolds for tissue engineering: a review, Macromol 3 (2023) 524-553.
- [16] B.A. Venmathi Maran, S. Jeyachandran, M. Kimura, A review on the electrospinning of polymer nanofibers and its biomedical applications, J. Compos. Sci. 8 (2024) 32.
- [17] A. Hiwrale, S. Bharati, P. Pingale, A. Rajput, Nanofibers: a current era in drug delivery system, Heliyon 9 (9) (2023) e18917.
- J. Yang, L. Xu, Electrospun nanofiber membranes with various structures for wound dressing, Materials 16 (17) (2023) 6021 (Basel).
- [19] L. Sethuram, J. Thomas, Therapeutic applications of electrospun nanofibers impregnated with various biological macromolecules for effective wound healing strategy – a review, Biomed. PharmacOther 157 (2023) 113996.
- [20] H. Zhang, X. Lin, X. Cao, Y. Wang, J. Wang, Y. Zhao, Developing natural polymers for skin wound healing, Bioact. Mater. 33 (2024) 355-376.
- [21] Y. Guo, D. Qiao, S. Zhao, P. Liu, F. Xie, B. Zhang, Biofunctional chitosan-biopolymer composites for biomedical applications, Mater. Sci. Eng. R: Rep. 159 (2024) 100775.
- J. Hu, Y. Lin, C. Cui, F. Zhang, T. Su, K. Guo, T. Chen, Clinical efficacy of wet dressing combined with chitosan wound dressing in the treatment of deep seconddegree burn wounds: a prospective, randomised, single-blind, positive control clinical trial, Int. Wound J. 20 (3) (2023) 699-705.
- S.M. Mawazi, M. Kumar, N. Ahmad, Y. Ge, S. Mahmood, Recent applications of chitosan and its derivatives in antibacterial, anticancer, wound healing, and tissue engineering fields, Polymers 16 (2024) 1351 (Basel).
- [24] B.S. Rajinikanth, DSR.K.K. Rajkumar, V. Vijayaragava, Chitosan-based biomaterial in wound healing: a review, Cureus 16 (2) (2024) e55193.
- V. Mikušová, P. Mikuš, Advances in chitosan-based nanoparticles for drug delivery, Int. J. Mol. Sci. 22 (17) (2021) 9652.
- G.C. Türkoğlu, N. Khomarloo, E. Mohsenzadeh, D.N. Gospodinova, M. Neznakomova, F. Salaün, PVA-based electrospun materials—a promising route to designing nanofiber mats with desired morphological shape—a review, Int. J. Mol. Sci. 25 (2024) 1668.
- [27] S.G. Jin, Production and application of biomaterials based on polyvinyl alcohol (PVA) as wound dressing, Chem. Asian J. 17 (21) (2022) e202200595.

 [28] F. Cialdai, C. Risaliti, M. Monici, Role of fibroblasts in wound healing and tissue
- remodeling on earth and in space, Front. Bioeng. Biotechnol. 10 (2022) 958381.
- G. Zhang, J. Li, D. Wang, H. Lou, C. Zhang, W. Liu, The mechanisms related to fibroblasts in burn surface, Skin Res. Technol. 29 (2023) 1-10.
- [30] B. Li, J.H.C. Wang, Fibroblasts and myofibroblasts in wound healing: force eneration and measurement, J. Tissue Viability. 20 (2011) 108–120.
- S. Sharma, V.K. Rai, R.K. Narang, T.S. Markandeywar, Collagen-based formulations for wound healing: a literature review, Life Sci. 290 (2022) 120096.
- [32] Z. Arezomand, S. Mashjoor, B.S. Makhmalzadeh, M.R. Shushizadeh, L. Khorsandi, Citrus flavonoids-loaded chitosan derivatives-route nanofilm as drug delivery systems for cutaneous wound healing, Int. J. Biol. Macromol. 271 (2024) 132670.
- J. Merl-Pham, T. Basak, L. Knüppel, D. Ramanujam, M. Athanason, J. Behr, S. Engelhardt, O. Eickelberg, S.M. Hauck, R. Vanacore, C.A. Staab-Weijnitz, Quantitative proteomic profiling of extracellular matrix and site-specific collagen post-translational modifications in an in vitro model of lung fibrosis, Matrix. Biol. Plus 1 (2019) 100005.
- [34] C. Ersanli, A. Tzora, I. Skoufos, C.C. Voidarou, D.I. Zeugolis, Recent advances in collagen antimicrobial biomaterials for tissue engineering applications: a review, Int. J. Mol. Sci. 24 (9) (2023) 7808.
- [35] M. Abinaya, M. Gayathri, Biodegradable collagen from scomberomorus lineolatus skin for wound healing dressings and its application on antibiofilm properties, J. Cell Biochem. 120 (9) (2019) 15572–15584.
- S.S. Mathew-Steiner, S. Roy, S.K. Sen, Collagen in wound healing, Bioengineering 8 (2021) 63 (Basel).
- [37] L. Bacakova, K. Novotna, D. Hadraba, J. Musilkova, P. Slepicka, M. Beran, Influence of biomimetically mineralized collagen scaffolds on bone cell proliferation and immune activation, Polymers 14 (2022) 602 (Basel).
- [38] M.C. Linju, M.R. Rekha, Proline conjugated chitosan as wound healing material: in vitro studies on the influence of the scaffold on collagen production and wound healing, Int. J. Biol. Macromol. 242 (2023) 124688.
- Z.Y. Tian, S. Wang, H. Lu, Hydroxyproline-derived biomimetic and biodegradable polymers, Cur. Opin. Solid State Mater. Sci. 25 (2021) 100902.

- [40] A. Miserez, J. Yu, P. Mohammadi, Protein-based biological materials: molecular design and artificial production, Chem. Rev. 123 (5) (2023) 2049–2111.
- [41] E. Kim, S. Ham, B.K. Jung, J.W. Park, J. Kim, J.H. Lee, Effect of baicalin on wound healing in a mouse model of pressure ulcers, Int. J. Mol. Sci. 24 (2023) 329.
- [42] G. Liu, Z. Bao, J. Wu, Injectable Baicalin/F127 hydrogel with antioxidant activity for enhanced wound healing, Chin. Chem. Lett. 31 (2020) 1817–1821.
- [43] W. Zeng, N.M. Cheng, X. Liang, H. Hu, F. Luo, J. Jin, Y.W. Li, Electrospun polycaprolactone nanofibrous membranes loaded with baicalin for antibacterial wound dressing, Sci. Rep. 12 (1) (2022) 10900.
- [44] A.K.M.H. Morshed, S. Paul, A. Hossain, T. Basak, M.S. Hossain, M.M. Hasan, M. A. Hasibuzzaman, T.I. Rahaman, M.A.R. Mia, P. Shing, M. Sohel, S. Bibi, D. Dey, P. Biswas, M.N. Hasan, L.C. Ming, C.S. Tan, Baicalein as promising anticancer agent: a comprehensive analysis on molecular mechanisms and therapeutic perspectives, Cancers 15 (7) (2023) 2128 (Basel).
- [45] W. Min, X. Liu, Q. Qian, B. Lin, D. Wu, M. Wang, I. Ahmad, N. Yusuf, D. Luo, Effects of Baicalin against UVA-induced photoaging in skin fibroblasts, Am. J. Chin. Med. 42 (3) (2014) 709–727.
- [46] Y. Wen, Y. Wang, C. Zhao, B. Zhao, J. Wang, The Pharmacological efficacy of baicalin in inflammatory diseases, Int. J. Mol. Sci. 24 (2023) 9317.
- [47] Z. Hu, Y. Guan, W. Hu, Z. Xu, M. Ishfaq, An overview of pharmacological activities of baicalin and its aglycone baicalein: new insights into molecular mechanisms and signaling pathways, Iran. J. Basic Med. Sci. 25 (2022) 14–26.
- [48] G. Jakab, D. Bogdán, K. Mazák, R. Deme, Z. Mucsi, I.M. Mándity, B. Noszál, N. Kállai-Szabó, Physicochemical profiling of baicalin along with the development and characterization of cyclodextrin inclusion complexes, AAPS PharmSciTech 20 (8) (2019) 314.
- [49] V. Rizzo, N. Ferlazzo, M. Currò, G. Isola, M. Matarese, M.P. Bertuccio, D. Caccamo, G. Matarese, R. Ientile, Baicalin-induced autophagy preserved lpsstimulated intestinal cells from inflammation and alterations of paracellular permeability, Int. J. Mol. Sci. 22 (2021) 2315.
- [50] S.X. Dai, Y. Zou, Y.L. Feng, H.B. Liu, X.B. Zheng, Baicalin down-regulates the expression of macrophage migration inhibitory factor (MIF) effectively for rats with ulcerative colitis, PhytOther Res. 26 (2012) 498–504.
- [51] F. Xing, W.J. Yi, F. Miao, M.Y. Su, T.C. Lei, Baicalin increases hair follicle development by increasing canonical Wnt/β-catenin signaling and activating dermal papillar cells in mice, Int. J. Mol. Med. 41 (2018) 2079–2085.
- [52] S. Werner, T. Krieg, H. Smola, Keratinocyte-fibroblast interactions in wound healing, J. Investig, Dermatol. 127 (2007) 998–1008.
- [53] S. Yan, Y. Wang, P. Liu, A. Chen, M. Chen, D. Yao, X. Xu, L. Wang, X. Huang, Baicalin attenuates hypoxia-induced pulmonary arterial hypertension to improve hypoxic cor pulmonale by reducing the activity of the p38 MAPK signaling pathway and MMP-9, Evid. Based Complement. Altern. Med. 2016 (2016) 2546402.
- [54] X. Sun, M. Pisano, L. Xu, F. Sun, J. Xu, W. Zheng, X. Liu, Y. Zhang, R. Sun, X. Cui, Baicalin regulates autophagy to interfere with small intestinal acute graft-versushost disease, Sci. Rep. 12 (2022) 6551.
- [55] J. Shen, J. Cheng, S. Zhu, J. Zhao, Q. Ye, Y. Xu, H. Dong, X. Zheng, Regulating effect of Baicalin on IKK/IKB/NF-kB signaling pathway and apoptosis-related proteins in rats with ulcerative colitis, Int. Immunopharmacol. 73 (2019) 193–200
- [56] B. Shen, H. Zhang, Z. Zhu, Z. Ling, F. Zeng, Y. Wang, J. Wang, Baicalin relieves LPS-induced lung inflammation via the NF-κB and MAPK pathways, Molecules 28 (2023) 1873
- [57] J. Feng, C. Guo, Y. Zhu, L. Pang, Z. Yang, Y. Zou, X. Zheng, Baicalin down regulates the expression of TLR4 and NFkB-p65 in colon tissue in mice with colitis induced by dextran sulfate sodium, Int. J. Clin. Exp. Med. 7 (2014) 4063–4072.
- [58] A.R. Hajipour, E. Boostani, F. Mohammadsaleh, Proline-functionalized Chitosan-palladium (II) complex, a Novel Nanocatalyst for C–C Bond Formation in Water, RSC Adv. 5 (31) (2015) 24742–24748.
- [59] P. Akay, D. Omay, Synthesis and characterization of chitosan and amino acid superabsorbent hydrogels, Int. Polym. Process. 29 (2) (2014) 287–294.
- [60] P. Tonglairoum, T. Ngawhirunpat, T. Rojanarata, S. Panomsuk, R. Kaomongkolgit, P. Opanasopit, Fabrication of mucoadhesive chitosan coated polyvinylpyrrolidone/cyclodextrin/clotrimazole sandwich patches for oral candidiasis, Carbohydr. Polym. 132 (2015) 173–179.
- [61] H. Ishii, M. Minegishi, B. Lavitpichayawong, T. Mitani, Synthesis of chitosanamino acid conjugates and their use in heavy metal uptake, Int. J. Biol. Macromol. 17 (1995) 21–23.
- [62] S. Jegina, L. Salaka, S. Kukle, D. Livkisa, J. Gravitis, A preliminary study on sodium hyaluronate loaded polyvinyl alcohol nanofiber webs obtained via roller electrospinning, IOP Conf. Ser. Mater. Sci. Eng. 500 (2019) 012024.
- [63] H.A. Joshi, R.S. Patwardhan, D. Sharma, S.K. Sandur, P.V. Devarajan, Pre-clinical evaluation of an innovative oral nano-formulation of baicalein for modulation of radiation responses, Int. J. Pharm. 595 (2021) 120181.
- [64] X. Wu, X. Deng, J. Wang, Q. Li, Baicalin inhibits cell proliferation and inflammatory cytokines induced by tumor necrosis factor α (TNF-α) in human immortalized keratinocytes (HaCaT) human keratinocytes by inhibiting the STAT3/nuclear factor kappa B (NF-κB) signaling pathway, Med. Sci. Monit. 26 (2020) e919392.
- [65] X. Diao, D. Yang, Y. Chen, W. Liu, Baicalin suppresses lung cancer growth by targeting PDZ-binding Kinase/T-LAK cell-originated protein kinase, Biosci. Rep. 39 (4) (2019) BSR20181692.
- [66] LY. Peng, M. Yuan, ZM. Wu, K. Song, C.L. Zhang, Q. An, F. Xia, J.L. Yu, P.F. Yi, B. D. Fu, H.Q. Shen, Anti-bacterial activity of baicalin against APEC through inhibition of quorum sensing and inflammatory responses, Sci. Rep. 9 (4063) (2019), https://doi.org/10.1038/s41598-019-40684-6.

- [67] P. Zou, W.H. Lee, Z. Gao, D. Qin, Y. Wang, J. Liu, T. Sun, Wound dressing from polyvinyl alcohol/chitosan electrospun fiber membrane loaded with OH-CATH30 nanoparticles, Carbohydr. Polym. 232 (2020) 115786.
- [68] A.R. Chandrasekaran, J. Venugopal, S. Sundarrajan, S. Ramakrishna, Fabrication of a nanofibrous scaffold with improved bioactivity for culture of human dermal fibroblasts for skin regeneration, Biomed. Mater. 6 (2011) 015001.
- [69] S. Mashjoor, M. Yousefzadi, M.A. Esmaeili, R. Rafiee, Cytotoxicity and antimicrobial activity of marine macro algae (dictyotaceae and ulvaceae) from the persian gulf, Cytotechnology 68 (2016) 1717–1726.
- [70] N. Gholipour, S. Mashjoor, M. Naderi, M.R. Pouyani, Z.E. Tubkanlu, N.M. Samaei, H. Khajeh, In vitro cytotoxic and apoptotic activities of allium paradoxum (M. Bieb.) G. Don extract on human breast cancer cell line, Indian J. Tradit. Knowl. 17 (2018) 247–254.
- [71] National Research Council (NRC), Guide for the Care and Use of Laboratory Animals, 8th ed., The National Academies Press, Washington, DC, 2011 https://doi.org/10.17226/12910.
- [72] American Veterinary Medical Association, AVMA guidelines on euthanasia, 2007 update, p 4–11. 2007. Available at http://www.avma.org/issues/animal_welfare/euthanasia.pdf.
- [73] S.V. Murphy, A. Skardal, L. Song, K. Sutton, R. Haug, D.L. Mack, J. Jackson, S. Soker, A. Atala, Solubilized amnion membrane hyaluronic acid hydrogel accelerates full-thickness wound healing, Stem Cells Transl. Med. 6 (2017) 2020–2032
- [74] Y. Yang, W. Xie, S. Li, X. Sun, B. Yu, H. Fu, M. Chen, Splint-free line drawing model: an innovative method for excisional wound models, Int. Wound J. 20 (2023) 2673–2678
- [75] A.K. Srivastava, P. Khare, H.K. Nagar, N. Raghuwanshi, R. Srivastava, Hydroxyproline: a potential biochemical marker and its role in the pathogenesis of different diseases, Curr. Protein Pept. Sci. 17 (6) (2016) 596–602.
- [76] J; He, C. Li, X. Cheng, Water soluble chitosan-amino Acid-BODIPY fluorescent probes for selective and sensitive detection of Hg²⁺/Hg⁺ Ions, Mater. Chem. Phys. 295 (2023) 127081.
- [77] T. Torkaman, H. Rahmani, A. Ashori, S.H. Mahmoudi Najafi, Modification of chitosan using amino acids for wound healing purposes: a review, Carbohydr. Polym. 258 (2021) 117675.
- Y. Zhong, E. Wei, L. Wu, Y. Wang, Q. Lin, N. Wu, H. Chen, Novel biomaterials for wound healing and tissue regeneration, ACS Omega 9 (30) (2024) 32268–32286.
 Y. Kusakabe, S.S. Moriya, T. Sugiyama, Y. Miyata, Isolation and identification of
- [79] Y. Kusakabe, S.S. Moriya, T. Sugiyama, Y. Miyata, Isolation and identification of the New Baicalin target protein to develop flavonoid structure-based therapeutic agents, Bioorg. Med. Chem. 90 (2023) 117362.
- [80] J.H. Lee, P. Parthiban, G.Z. Jin, J.C. Knowles, H.W. Kim, Materials roles for promoting angiogenesis in tissue regeneration, Prog. Mater. Sci. 177 (2021) 100732.
- [81] S. Jin, J. Gao, R. Yang, C. Yuan, R. Wang, Q. Zou, Y. Zuo, M. Zhu, Y. Li, Y. Man, J. Li, A Baicalin-loaded coaxial nanofiber scaffold regulated inflammation and osteoclast differentiation for vascularized bone regeneration, Bioact. Mater. 8 (2021) 559–572.
- [82] R. Xu, H. Xia, W. He, Z. Li, J. Zhao, B. Liu, Y. Wang, Q. Lei, Y. Kong, Y. Bai, Z. Yao, Y. Yan, H. Li, R. Zhan, S. Yang, G. Luo, J. Wu, Controlled water vapor transmission rate promotes wound-healing via wound re-epithelialization and contraction enhancement, Sci. Rep. 6 (2016) 24596.
- [83] L.L. Lima, T.B. Taketa, M.M. Beppu, I.M.O. Sousa, M.A. Foglio, A.M. Moraes, Coated electrospun bioactive wound dressings: mechanical properties and ability to control lesion microenvironment, Mater. Sci. Eng. C 100 (2019) 493–504.
- [84] Q. Luo, J. Hong, H. Xu, S. Han, H. Tan, Q. Wang, J. Tao, N. Ma, Y. Cheng, H. Su, Hygroscopicity of amino acids and their effect on the water uptake of ammonium sulfate in the mixed aerosol particles, Sci. Total. Environ. 734 (2020) 139318.
- [85] S. Rýglová, M. Braun, T. Suchý, Collagen and its modifications—crucial aspects with concern to its processing and analysis, Macromol. Mater. Eng. 302 (6) (2017) 1600460.
- [86] I.M. Yermak, V.N. Davydova, A.V. Volod'ko, Mucoadhesive marine polysaccharides, Mar. Drugs 20 (2022) 522.
- [87] P. Mura, F. Maestrelli, M. Cirri, N. Mennini, Multiple roles of chitosan in mucosal drug delivery: an updated review, Mar. Drugs 20 (5) (2022) 335.
- [88] W. Dong, J. Ye, J. Zhou, W. Wang, H. Wang, X. Zheng, Y. Yang, X. Xia, Y. Liu, Comparative study of mucoadhesive and mucus-penetrative nanoparticles Based on phospholipid complex to overcome the mucus barrier for inhaled delivery of baicalein, Acta Pharm. Sin. B 10 (8) (2020) 1576–1585.
- [89] K. Li, Y. Liang, A. Cheng, Q. Wang, Y. Li, H. Wei, C. Zhou, X. Wan, Antiviral properties of baicalin: a concise review, Rev. Bras. Farmacogn. 31 (4) (2021) 408–419.
- [90] J. Luan, F. Zheng, X. Yang, A. Yu, G. Zhai, Nanostructured lipid carriers for oral delivery of baicalin: in vitro and in vivo evaluation, Colloids Surf. A Physicochem. Eng. Asp. 466 (2015) 154–159.
- [91] K. Noh, Y. Kang, M.R. Nepal, K.S. Jeong, D.G. Oh, M.J. Kang, S. Lee, W. Kang, H. G. Jeong, T.C. Jeong, Role of intestinal microbiota in baicalin-induced drug interaction and its pharmacokinetics, Molecules 21 (2016) 337.
- [92] K. Sato, T.T. Asai, S. Jimi, Collagen-derived di-peptide, prolylhydroxyproline (Pro-Hyp): a new low molecular weight growth-initiating factor for specific fibroblasts associated with wound healing, Front. Cell Dev. Biol. 8 (2020) 548075
- [93] X. Wang, J. Li, X. Lin, Y. Zhang, The s-oph enzyme for efficient degradation of polyvinyl alcohol: soluble expression and catalytic properties, Mol. Biol. Rep. 50 (2023) 8523–8535.

- [94] M. Ahmad, C. Ritzoulis, W. Pan, J. Chen, Biologically-relevant interactions, phase separations and thermodynamics of chitosan–mucin binary systems, Process. Biochem. 94 (2020) 152–163.
- [95] D.L. Roman, V. Ostafe, A. Isvoran, Deeper inside the specificity of lysozyme when degrading chitosan. A structural bioinformatics study, J. Mol. Graph. Model. 100 (2020) 107676.
- [96] M.K. Amin, J.S. Boateng, Enhancing stability and mucoadhesive properties of chitosan nanoparticles by surface modification with sodium alginate and polyethylene glycol for potential oral mucosa vaccine delivery, Mar. Drugs 20 (2022) 156.
- [97] R. Wibel, D.E. Braun, L. Hämmerle, A.M. Jörgensen, P. Knoll, W. Salvenmoser, C. Steinbring, A. Bernkop-Schnürch, In vitro investigation of thiolated chitosan derivatives as mucoadhesive coating materials for solid lipid nanoparticles, Biomacromolecules 22 (9) (2021) 3980–3991.
- [98] Y. Zhu, L. Zhang, L. Zhou, X. Li, Y. Zhao, J. Wang, Investigation on baicalin-loaded chitosan film crosslinked by graphene oxide and its biocompatibility, Biosurf. Biotribol. 9 (2) (2023) 35–44.
- [99] Y. Li, Z.D. He, Q.E. Zheng, C. Hu, W.F. Lai, Hydroxypropyl-_cyclodextrin for delivery of baicalin via inclusion complexation by supercritical fluid encapsulation, Molecules 23 (5) (2018) 1169.
- [100] L. Cui, E. Sune, J. Song, J. Wang, X.B. Jia, Z.H. Zhang, Characterization and bioavailability study of baicalin-mesoporous carbon nanopowder solid dispersion, Pharmacogn. Mag. 12 (48) (2016) 326–332.
- [101] G.S.A. Suleiman, X. Zeng, R. Chakma, I.Y. Wakai, Y. Feng, Recent advances and challenges in thermal stability of PVA-based film: a review, Appl. Res. 32 (2) (2024) e6327
- [102] D.V. Bhalani, B. Nutan, A. Kumar, A.K. Singh Chandel, Bioavailability enhancement techniques for poorly aqueous soluble drugs and therapeutics, Biomedicines 10 (9) (2022) 2055.
- [103] Z. Feng, J. Zhou, X. Shang, G. Kuang, J. Han, L. Lu, L. Zhang, Comparative research on stability of baicalin and baicalein administrated in monomer and total flavonoid fraction form of radix scutellariae in biological fluids in vitro, Pharm. Biol. 55 (1) (2017) 1177–1184.
- [104] Y. Herdiana, N. Wathoni, S. Shamsuddin, M. Muchtaridi, Drug release study of the chitosan-based nanoparticles, Heliyon 8 (1) (2022) e08674.
- [105] R.I. El-Gogary, S.A.A. Gaber, M. Nasr, Polymeric nanocapsular baicalin: chemometric optimization, physicochemical characterization and mechanistic anticancer approaches on breast cancer cell lines, Sci. Rep. 9 (2019) 11064.
- [106] L. Guo, M. Han, H. Zhang, Y. Han, Effect of chitosan/dioleyl phosphatidyl ethanolamine - Baicalein nanohydrogel in the treatment of rat with periodontitis, Heliyon 10 (3) (2024) e25209.
- [107] J. Yang, A. Chen, X. He, S. Lu, Fabrication of baicalein-encapsulated zeolitic imidazole framework as a novel nanocomposited wound closure material to persuade pH-responsive healing efficacy in post-caesarean section wound care, Int. Wound J. 20 (6) (2023) 1921–1933.
- [108] R.T. Stiepel, E.S. Pena, S.A. Ehrenzeller, M.D. Gallovic, L.M. Lifshits, C.J. Genito, E.M. Bachelder, K.M. Ainslie, A predictive mechanistic model of ddrug release from surface eroding polymeric nanoparticles, J. Control Release 351 (2022) 883–895.
- [109] Y. Wei, J. Guo, X. Zheng, J. Wu, Y. Zhou, Y. Yu, Y. Ye, L. Zhang, L. Zhao, Y. Zou, W. Zheng, H. Liu, Pharmacokinetics and biodistribution of baicalin-loaded liposomes, Int. J. Nanomedicine 9 (1) (2014) 3623–3630.
- [110] G. Wenjuan, Y. Jie, D. Zhao, H. Weizhao, A new method for enriching baicalin in scutellaria baicalensis georgi by metal organic framework material ZIF-8, Acta Chim. Sin. 77 (11) (2019) 1203–1210.
- [111] L. Huang, X.H. Huang, X. Yang, J.Q. Hu, Y.Z. Zhu, P.Y. Yan, Y. Xie, Novel nano-drug delivery system for natural products and their application, Pharmacol. Res. 201 (2024) 107100
- [112] S. Qin, X. Huang, S. Qu, Baicalin induces a potent innate immune response to inhibit respiratory syncytial virus replication via regulating viral non-structural 1 and matrix RNA, Front. Immunol. 13 (2022) 907047.
- [113] H. Yang, J. Wang, Q. Tan, Z. Dong, Z. Yang, P. Zhang, W. Wang, Supramolecular interaction between berberine hydrochloride and baicalin in aqueous solution: reaction kinetics, spectral analysis and dynamic simulation, Heliyon 10 (9) (2024) e29992.
- [114] R. Liu, X. Li, J. Wei, S. Liu, Y. Chang, J. Zhang, J. Zhang, X. Zhang, U. Fuhr, M. Taubert, X. Tian, A single dose of baicalin has no clinically significant effect on the pharmacokinetics of cyclosporine a in healthy chinese volunteers, Front. Pharmacol. 10 (2019) 518.
- [115] M.J.C. Im, J.E. Hoopes, Enzyme activities in regenerating epithelium during wound healing: II. β-Glucuronidase, J. Surg. Res. 12 (2) (1972) 406–410.
- [116] Y. Tang, H. Zhu, Y. Zhang, C. Huang, Determination of human plasma protein binding of baicalin by ultrafiltration and high-performance liquid chromatography, Biomed. Chromatogr. 20 (2006) 1116–1119.

- [117] M.H. Perruchot, F. Gondret, F. Robert, E. Dupuis, H. Quesnel, F. Dessauge, Effect of the favonoid baicalin on the proliferative capacity of bovine mammary cells and their ability to regulate oxidative stress, Peer J. 7 (2019) e6565.
- [118] J. Chen, C. Lin, X. Huang, B. Wei, Baicalin enhances proliferation and reduces inflammatory-oxidative stress effect in H₂O₂-induced granulosa cells apoptosis via USP48 protein regulation, BMC Complement. Med. Ther. 24 (2024) 42, https://doi.org/10.1186/s12906-024-04346-z.
- [119] Y. Chen, M. Shafiq, M. Liu, Y. Morsi, X. Mo, Advanced fabrication for electrospun three-dimensional nanofiber aerogels and scaffolds, Bioact. Mater. 5 (4) (2020) 963–979.
- [120] X. Zhao, Q. Li, Z. Guo, Z. Li, Constructing a cell microenvironment with biomaterial scaffolds for stem cell therapy, Stem Cell Res. Ther. 12 (1) (2021) 583
- [121] H. Richards, S. Falder, PH of a burn wound, Burn 44 (8) (2018) 2104-2105.
- [122] N. Aibani, R. Rai, P. Patel, G. Cuddihy, E.K. Wasan, Chitosan nanoparticles at the biological interface: implications for drug delivery, Pharmaceutics 13 (10) (2021) 1686
- [123] D. Ribble, N.B. Goldstein, D.A. Norris, Y.G. Shellman, A simple technique for quantifying apoptosis in 96-well plates, BMC Biotechnol. 5 (2005) 12.
- [124] L.C. Crowley1, B.J. Marfell, N.J. Waterhouse, Analyzing cell death by nuclear staining with hoechst 33342, Cold. Spring. Harb. Protoc. 9 (2016) 778–781.
- [125] E. Karna, L. Szoka, T.Y.L. Huynh, J.A. Palka, Proline-dependent regulation of collagen metabolism, Cell Mol. Life Sci. 77 (10) (2020) 1911–1918.
- [126] G. Wu, F.W. Bazer, R.C. Burghardt, G.A. Johnson, S.W. Kim, D.A. Knabe, P. Li, X. Li, J.R. McKnight, M.C. Satterfield, T.E. Spencer, Proline and hydroxyproline metabolism: implications for animal and human nutrition, Amino Acids 40 (2011) 1053–1063.
- [127] J. Roman, Fibroblasts—warriors at the intersection of wound healing and disrepair, Biomolecules 13 (2023) 945.
- [128] X. Sun, X. Cui, X. Chen, X. Jiang, Baicalein alleviated TGF β1-induced type I collagen production in lung fibroblasts via downregulation of connective tissue growth factor, Biomed. PharmacOther 131 (2020) 110744.
- [129] J. Witowski, A. Thiel, R. Dechend, K. Dunkel, N. Fouquet, T.O. Bender, J. M. Langrehr, G.M. Gahl, U. Frei, A. Jörres, Synthesis of C-X-C and C-C chemokines by human peritoneal fibroblasts: induction by macrophage-derived cytokines, Am. J. Pathol. 158 (2001) 1441–1450.
- [130] D. Correa-Gallegos, D. Jiang, Y. Rinkevich, Fibroblasts as confederates of the immune system, Immunol. Rev. 302 (2021) 147–162.
- [131] L. Che, R. Mirza, Y. Kwon, L.A. DiPietro, T.J. Koh, The murine excisional wound model: contraction revisited, Wound Repair. Regen. 23 (2015) 874–877.
- [132] M.O. Ilomuanya, P.S. Okafor, J.N. Amajuoyi, J.C. Onyejekwe, O.O. Okubanjo, S. O. Adeosun, B.O. Silva, Polylactic acid-based electrospun fiber and hyaluronic acid-valsartan hydrogel scaffold for ch,ronic wound healing, Beni-Suef Univ. J. Basic Appl. Sci. 9 (2020) 31, https://doi.org/10.1186/s43088-020-00057-9.
- [133] W. Zhang, S. Zhao, S. Wu, T. Song, Q. Guan, J. Xu, J. Wang, P. Li, Y. Fan, A multifunctional baicalin-coordinated borate ions/bacterial cellulose composite hydrogel for efficient treatment of chronic wounds, Med. Nov. Technol. Devices 23 (2024) 100315
- [134] M. Manconi, M.L. Manca, C. Caddeo, C. Cencetti, C.D. Meo, N. Zoratto, A. Nacher, A.M. Fadda, P. Matricardi, Preparation of gellan-cholesterol nanohydrogels embedding baicalin and evaluation of their wound healing activity, Eur. J. Pharm. Biopharm. 127 (2018) 244–249.
- [135] L. Qian, K. Yang, X. Liu, L. Zhang, H. Zhao, L.Z. Qiu, Y. Chu, W. Hao, Y. Zhuang, Y. Chen, J. Da, Baicalein-functionalized collagen scaffolds direct neuronal differentiation toward enhancing spinal cord injury repair, Biomater. Sci. 11 (2023) 678–689.
- [136] M.M. Islam, M. Shahruzzaman, S. Biswas, M. Nurus Sakib, T.U. Rashid, Chitosan based bioactive materials in tissue engineering applications-a review, Bioact. Mater. 5 (2020) 164–183.
- [137] G.S. Schultz, G.A. Chin, L. Moldawer, R.F. Diegelmann, Principles of wound healing, Fitridge R, Thompson M, editors, in: Mechanisms of Vascular Disease: A Reference Book for Vascular Specialists, 23, University of Adelaide Press, Adelaide (AU), 2011, https://www.ncbi.nlm.nih.gov/books/NBK534261/.
- [138] P. Rousselle, F. Braye, G. Dayan, Re-epithelialization of adult skin wounds: cellular mechanisms and therapeutic strategies, Adv. Drug Deliv. Rev. 146 (2019) 344–365.
- [139] V.L. Albaugh, K. Mukherjee, A. Barbul, Proline precursors and collagen synthesis: biochemical challenges of nutrient supplementation and wound healing, J. Nutr. 147 (11) (2017) 2011–2017.
- [140] L.A. Lifshits, M. Rabin, R. Tohar, F. Netti, M. Gabay, M. Sova, D.Z. Bar, E. Weinberg, A. Adler-Abramovich, M. Gal, Enhancement of collagen-i levels in human gingival fibroblasts by small molecule activation of HIF-1α, J. Agric. Food Chem. 71 (20) (2023) 7829–7835.